JOURNAL OF GEOPHYSICAL RESEARCH: SOLID EARTH, VOL. 118, 138–164, doi:10.1029/2012JB009721, 2013

Global observation of vertical-CLVD earthquakes at active volcanoes

Ashley Shuler,[1,2,3] Meredith Nettles,[1,2] and Göran Ekström[1,2]

Received 24 August 2012; revised 29 November 2012; accepted 4 December 2012; published 27 January 2013.

[1] Some of the largest and most anomalous volcanic earthquakes have non-double-couple focal mechanisms. Here, we investigate the link between volcanic unrest and the occurrence of non-double-couple earthquakes with dominant vertical tension or pressure axes, known as vertical compensated-linear-vector-dipole (vertical-CLVD) earthquakes. We determine focal mechanisms for 313 target earthquakes from the standard and surface wave catalogs of the Global Centroid Moment Tensor Project and identify 86 shallow $4.3 \leq M_W \leq 5.8$ vertical-CLVD earthquakes located near volcanoes that have erupted in the last ~100 years. The majority of vertical-CLVD earthquakes occur in subduction zones in association with basaltic-to-andesitic stratovolcanoes or submarine volcanoes, although vertical-CLVD earthquakes are also located in continental rifts and in regions of hot spot volcanism. Vertical-CLVD earthquakes are associated with many types of confirmed or suspected eruptive activity at nearby volcanoes, including volcanic earthquake swarms as well as effusive and explosive eruptions and caldera collapse. Approximately 70% of all vertical-CLVD earthquakes studied occur during episodes of documented volcanic unrest at a nearby volcano. Given that volcanic unrest is underreported, most shallow vertical-CLVD earthquakes near active volcanoes are likely related to magma migration or eruption processes. Vertical-CLVD earthquakes with dominant vertical pressure axes generally occur after volcanic eruptions, whereas vertical-CLVD earthquakes with dominant vertical tension axes generally occur before the start of volcanic unrest. The occurrence of these events may be useful for identifying volcanoes that have recently erupted and those that are likely to erupt in the future.

Citation: Shuler, A., M. Nettles, and G. Ekström (2013), Global observation of vertical-CLVD earthquakes at active volcanoes, *J. Geophys. Res. Solid Earth*, *118*, 138–164, doi:10.1029/2012JB009721.

1. Introduction

[2] Most shallow earthquakes have seismic radiation patterns that are consistent with the double-couple model for shear failure on planar faults [*Sykes*, 1967; *Isacks et al*., 1968; *Dziewonski and Woodhouse*, 1983; *Frohlich*, 1995]. However, in volcanic and geothermal areas, other processes such as the migration of magmatic and/or hydrothermal fluids or rupture on non-planar faults can produce earthquakes with significant non-double-couple components. Although the majority of these anomalous earthquakes are small ($M < 3$) and only recorded by seismometers deployed close to the source regions [*Takeo*, 1990; *Foulger and Julian*, 1993; *Ross et al*., 1996; *Miller et al*., 1998a, 1998b; *Ohminato et al*., 1998, 2006; *Foulger et al*., 2004; *Kumagai et al*., 2005; *Nakano and Kumagai*, 2005; *Ohminato*, 2008], non-double-couple earthquakes with magnitudes up to $M \sim 6$ have been observed near a small number of volcanoes around the world [*Julian*, 1983; *Julian and Sipkin*, 1985; *Kanamori et al*., 1993; *Ekström*, 1994; *Dziewonski et al*., 1997; *Nettles and Ekström*, 1998; *Dreger et al*., 2000; *Kumagai et al*., 2001; *Templeton and Dreger*, 2006; *Minson and Dreger*, 2008; *Shuler and Ekström*, 2009].

[3] In this study, we investigate a specific type of non-double-couple earthquake that has been shown to occur near volcanic centers [*Ekström*, 1994]. Notable examples of these "vertical-CLVD" earthquakes include the 1984 Tori Shima earthquake [*Kanamori et al*., 1993] and the two series of earthquakes that occurred near Bárdarbunga volcano between 1976 and 1996 [*Nettles and Ekström*, 1998] and near Nyiragongo volcano between 2002 and 2005 [*Shuler and Ekström*, 2009]. In addition to having anomalous source properties, these earthquakes are associated with documented episodes of volcanic unrest, and their occurrence and unusual focal mechanisms are interpreted to result from active volcanic processes. However, it is not clear how widespread the association between vertical-CLVD earthquakes and active volcanism may be.

All Supporting Information may be found in the online version of this article.

[1]Lamont-Doherty Earth Observatory, Columbia University, New York, New York, USA.
[2]Department of Earth and Environmental Sciences, Columbia University, New York, New York, USA.
[3]Now at Department of Earth and Planetary Sciences, University of California Santa Cruz, Santa Cruz, California, USA.

Corresponding author: A. Shuler, Department of Earth and Planetary Sciences, University of California Santa Cruz, 1156 High St., Santa Cruz, CA 95064, USA. (ashuler@ucsc.edu)

2169-9313/13/2012JB009721

[4] The focal mechanisms for earthquakes like those observed at Tori Shima, Bárdarbunga, and Nyiragongo have unusually large non-double-couple components. The size of the non-double-couple component is typically quantified by examination of the eigenvalues of the moment tensor. In the principal axis coordinate system, earthquakes are described by three eigenvectors with eigenvalues ordered $\lambda_1 \geq \lambda_2 \geq \lambda_3$, where λ_1 is the tension axis and λ_3 is the pressure axis. For double-couple earthquakes, the value of the intermediate eigenvalue, λ_2, is zero and $\lambda_3 = -\lambda_1$, whereas for non-double-couple earthquakes, λ_2 assumes a non-zero value due to isotropic or compensated-linear-vector-dipole (CLVD) components of the moment tensor [*Knopoff and Randall*, 1970; *Frohlich*, 1990a; *Julian et al*., 1998]. The isotropic component, $(M_{rr}+M_{\theta\theta}+M_{\phi\phi})/3$, represents a net volume change, which is expected to be small for tectonic earthquakes. In routine moment-tensor inversions, the isotropic component is typically constrained to be zero [*Dziewonski et al*., 1981; *Dufumier and Rivera*, 1997]. The CLVD component describes the portion of the moment tensor that can be explained by three orthogonal dipoles, two that have the same polarity and magnitude and a third that is twice as large with opposite polarity.

[5] The deviatoric component of the moment tensor can be decomposed into double-couple and CLVD components by assuming that the principal stress axes for these components are parallel. The non-double-couple component is described by the parameter ε, which is defined as

$$\varepsilon = -\lambda_2 / \max(|\lambda_1|, |\lambda_3|), \quad (1)$$

where $\varepsilon = 0$ for double-couple earthquakes and $\varepsilon = \pm 0.5$ for earthquakes that are pure CLVDs. In this framework, each earthquake can be described by a deviatoric moment tensor that is 200*|ε|% non-double-couple and (100–200*|ε|)% double couple. In the Global Centroid Moment Tensor (GCMT) catalog, ~18% of earthquakes with centroid depths less than 50 km have moment tensors with 40% or more non-double-couple component.

[6] In this paper, we focus on vertical-CLVD earthquakes, which have large non-double-couple components and approximately vertical dominant pressure or tension axes like those previously reported at active volcanoes [*Kanamori et al*., 1993; *Ekström*, 1994; *Nettles and Ekström*, 1998; *Shuler and Ekström*, 2009]. We identify two types of vertical-CLVD earthquakes depending on whether the dominant dipole is dilatational or compressional. "Vertical-T" earthquakes have dominant tension axes that plunge more steeply than 60° with $\varepsilon > 0.20$, and "vertical-P" earthquakes have dominant pressure axes that plunge more steeply than 60° with $\varepsilon < -0.20$ (Figure 1). Our definitions are similar, but not identical, to the P_V and T_V designations given by *Frohlich* [1995]. Earthquakes meeting our criteria represent less than 3% of all shallow ($h < 50$ km) earthquakes documented in the GCMT catalog.

[7] *Ekström* [1994] performed a search for vertical-T earthquakes in the Harvard CMT catalog (now known as the GCMT catalog) and identified 18 shallow $M_W > 5.0$ earthquakes with $\varepsilon > 0.33$ and tension axes that plunge more steeply than 60°. Ten of the vertical-T earthquakes are located in close proximity to volcanic centers, which demonstrates an association between these earthquakes and volcanism. Vertical-T earthquakes reported by *Ekström* [1994] include the Tori Shima earthquake and six Bárdarbunga earthquakes in addition to events in North Honshu, the Volcano Islands, and the South Sandwich Islands.

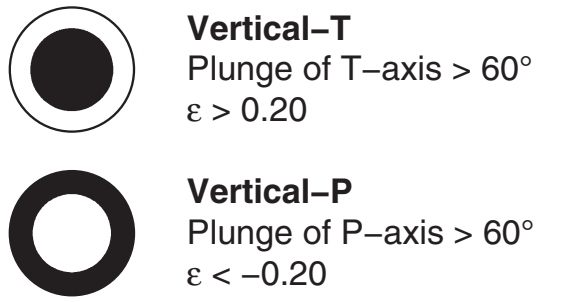

Figure 1. Criteria for the two types of vertical-CLVD earthquakes. Vertical-T events have dominant tension axes that plunge more steeply than 60° and ε values greater than 0.20, and vertical-P events have dominant pressure axes that plunge more steeply than 60° and ε values less than −0.20. The focal mechanisms shown are for pure vertical-CLVD earthquakes, which have vertical dominant tension or pressure axes (plunges of 90°) and $|\varepsilon| = 0.50$.

[8] The Tori Shima earthquake is an M_W 5.6 vertical-T earthquake that occurred on 13 June 1984 between Smith Rock and Bayonnaise Rocks volcanoes in the Izu-Bonin volcanic arc southeast of Honshu. In the GCMT catalog, the Tori Shima earthquake has an ε value of 0.33 and a tension axis that plunges 87°. Rayleigh waves from this earthquake were radiated with nearly equal amplitude and phase in all directions, whereas Love waves were either absent or of very low amplitude [*Kanamori et al*., 1993]. The Tori Shima earthquake also generated a disproportionately large tsunami given its moderate magnitude. Whereas typically tsunamis have tsunami magnitudes, M_t, that are comparable to the M_W estimates for the source earthquake, the Tori Shima earthquake produced an M_t 7.3 tsunami [*Abe*, 1988; *Satake and Kanamori*, 1991].

[9] Several physical mechanisms have been proposed to explain the Tori Shima earthquake. In the model of *Kanamori et al*. [1993], the vertical-T earthquake is generated by rapid expansion of supercritical water following horizontal injection of magma into water-filled sediments. However, *Ekström* [1994] suggests that the Tori Shima earthquake may be better explained by dip-slip motion on a volcano ring fault. Ring-fault structures are observed in eroded volcanoes [*Cole et al*., 2005 and references therein], and their presence can be inferred beneath some active volcanoes from dense cone-shaped patterns of microearthquakes [*Mori and McKee*, 1987; *Mori et al*., 1996]. In analog and numerical models, slip on ring-fault structures is directly related to the inflation or deflation of shallow magma chambers (see *Marti et al*., [2008], *Acocella* [2008] and *Gudmundsson* [2008] for review). Dip-slip motion on cone-shaped ring faults can generate earthquakes with vertical-CLVD focal mechanisms [*Frohlich*, 1989; *Frohlich*, 1990a, 1990b, 1995; *Ekström*, 1994; *Julian et al*., 1998], and slip on curved faults results in the partial cancelation of long-period seismic moment,

which could account for the discrepancy between seismic and tsunami magnitudes [*Ekström*, 1994].

[10] The non-double-couple earthquakes at Bárdarbunga and Nyiragongo volcanoes have also been explained as resulting from slip on ring-fault structures. In total, 10 vertical-T earthquakes with magnitudes $5.1 \leq M_W \leq 5.6$ occurred near Bárdarbunga volcano in Iceland between 1976 and 1996 [*Nettles and Ekström*, 1998]. The last earthquake occurred only ~1.5 days before a large, subglacial fissure eruption was observed between Bárdarbunga and Grimsvötn volcanoes [*Gudmundsson et al*., 1997]. The spatial and temporal relationship between the occurrence of the last vertical-T event and the start of the 1996 eruption suggests that vertical-T earthquakes at Bárdarbunga may be associated with the inflation of a shallow magma chamber. According to the faulting model presented by *Nettles and Ekström* [1998], the 10 vertical-T earthquakes are generated by slip on an outward-dipping ring fault located below an inflating shallow magma chamber.

[11] Five vertical-P earthquakes with magnitudes $4.6 \leq M_W \leq 5.3$ took place near Nyiragongo volcano in the Democratic Republic of the Congo between 2002 and 2005. The first three vertical-P earthquakes occurred several days after a fissure eruption of Nyiragongo in January 2002 and are attributed to slip on inward-dipping ring faults located above a deflating shallow magma chamber [*Shuler and Ekström*, 2009]. The final two earthquakes occurred in 2003 and 2005 as the lava lake in Nyiragongo's summit crater refilled and are explained as slip on a deeper inward-dipping ring fault triggered by the upward flux of magma into shallow levels of the magmatic plumbing system.

[12] Although there is still controversy over the physical mechanisms that generate vertical-CLVD earthquakes [e.g., *Konstantinou et al*., 2003; *Tkalčić et al*., 2009; *Fichtner and Tkalčić*, 2010], the Tori Shima, Bárdarbunga, and Nyiragongo events illustrate that vertical-CLVD earthquakes are closely linked to dynamic processes occurring inside volcanic systems. The Tori Shima and Bárdarbunga events suggest that, in some cases, vertical-CLVD earthquakes may be triggered by the ascent of magma through the shallow crust, and the occurrence of these earthquakes may signal that a nearby volcano is likely to erupt in the future. The Nyiragongo events suggest that some vertical-CLVD earthquakes may be a response to magma migration, which would make these earthquakes useful for identifying the locations of recent eruptions.

[13] In this study, we explore the relationship between vertical-CLVD earthquakes and volcanic unrest. Using two global seismicity catalogs and seismic data from many regional and global seismic networks, we perform a systematic global search for additional examples of moderate-sized vertical-CLVD earthquakes located near active volcanoes. We quantify where and how often vertical-CLVD earthquakes occur near these volcanoes and investigate whether vertical-CLVD earthquakes are preferentially associated with particular tectonic settings or categories of volcanoes, or with specific types of eruptive activity. We characterize these earthquakes and document their relationships to volcanic unrest in detail in an effort to learn how vertical-CLVD earthquakes are linked to active deformation and eruption processes. A companion paper (A. Shuler et al., Physical mechanisms for vertical-CLVD earthquakes at active volcanoes, submitted to *Journal of Geophysical Research,* 2012) investigates the physical mechanisms that may be responsible for generating vertical-CLVD earthquakes at volcanoes.

2. Data and Methods

[14] We search for vertical-CLVD earthquakes near volcanoes using two catalogs from the Global CMT Project (www.globalcmt.org). The first catalog is the standard GCMT catalog [*Dziewonski et al*., 1981; *Ekström et al*., 2012], which contains centroid times, locations, and moment tensors for over 30,000 earthquakes since 1976. We investigate target earthquakes that have centroid locations near volcanoes and vertical-CLVD moment tensors in the GCMT catalog. To identify those earthquakes that have robust vertical-CLVD focal mechanisms, we recalculate CMT solutions for target earthquakes using additional data and updated methodology. The second catalog is the Surface Wave catalog, which contains epicenters, times, and magnitude estimates for earthquakes that are detected and located using intermediate-period surface waves following the method of *Ekström* [2006]. Although the Surface Wave catalog has documented approximately 2000 shallow earthquakes each year since 1991, we only investigate those earthquakes occurring near volcanoes. We examine two subsets of target earthquakes: earthquakes that were not reported in other seismicity catalogs and earthquakes with surface-wave magnitudes significantly larger than magnitudes reported elsewhere. We calculate CMT solutions for these earthquakes in the same manner as for events from the GCMT catalog. We also model teleseismic body waves to confirm the shallow depths of earthquakes we find to have vertical-CLVD focal mechanisms.

2.1. Selection of Target Earthquakes

[15] In order to assess the link between vertical-CLVD earthquakes and volcanic unrest, we investigate target earthquakes from the GCMT and Surface Wave catalogs that are located within 100 km of a recently active volcano. We restrict our search to the 429 D1 and D2 volcanoes in the Smithsonian Institution's Global Volcanism Program (GVP) database [*Siebert and Simkin*, 2002-], which have last known eruptions later than 2000 and 1900, respectively. This list is biased toward subaerial eruptions and represents only a fraction of volcanoes that are active or potentially active worldwide. However, since our primary goal is to explore the relationships between vertical-CLVD earthquakes and active volcanic processes, we limit our scope to those volcanoes with recently documented eruptions. The distance threshold of 100 km accounts for the uncertainty in locations from the GCMT [*Smith and Ekström*, 1997; *Hjörleifsdóttir and Ekström*, 2010] and Surface Wave catalogs, as well as the size and spacing of volcanic centers [*de Bromand d'Ars et al*., 1995; *Schmincke*, 2004]. A map of the recently active volcanoes and the target earthquakes is shown in Figure 2.

2.1.1. The Global CMT Catalog (1976–2009)

[16] The GCMT catalog contains moment tensor and location information for most earthquakes larger than M_W 5.0–5.5 since 1976 [*Dziewonski et al*., 1981; *Ekström et al*., 2012]. The vast majority of GCMT solutions are calculated using initial hypocentral parameters provided by the National Earthquake Information Center (NEIC) of the United States Geological Survey (USGS) and long-period

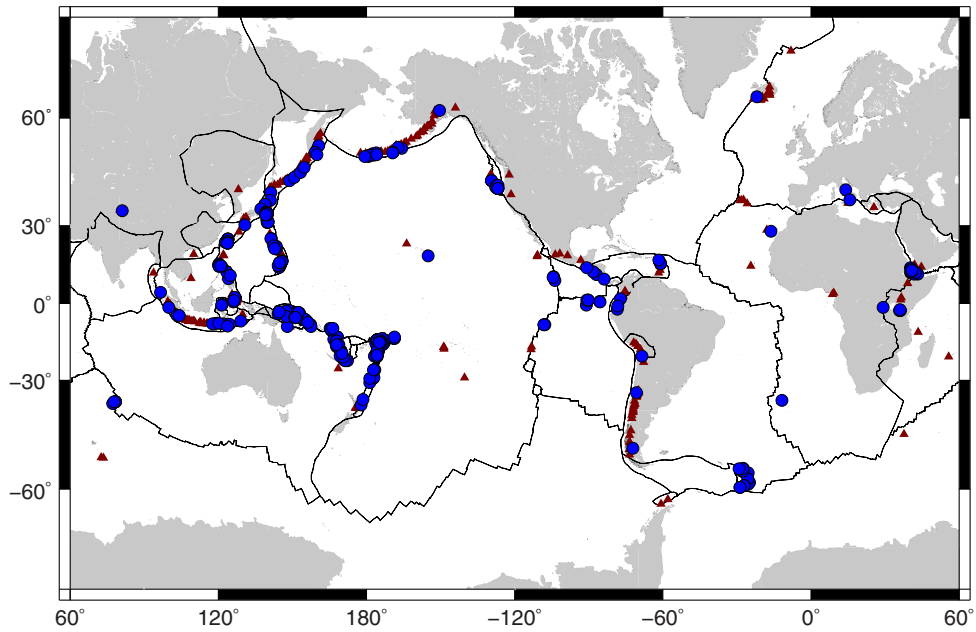

Figure 2. Map showing the locations of the 429 recently active volcanoes (maroon triangles) and 395 target earthquakes (blue circles) studied here. The volcanoes have last known eruptions later than 1900. The target earthquakes include 135 earthquakes from the Global CMT catalog and 261 earthquakes from the Surface Wave catalog (71 and 190 earthquakes from Category 1 and Category 2, respectively). Category 1 earthquakes are reported in the ISC catalog, but have surface-wave magnitudes, M_{SW} [*Ekström*, 2006], that are at least one magnitude unit larger than the m_b estimates provided by the ISC. Category 2 earthquakes are newly detected earthquakes that were detected and located using intermediate-period surface waves [*Ekström*, 2006], but which are missing from the ISC and NEIC bulletins. An earthquake on 26 May 2009 is a Category 1 earthquake that is also described in the GCMT catalog. Plate boundaries are from *Bird* [2003].

data primarily recorded on the IRIS-USGS Global Seismographic Network (GSN) or its historical equivalent. Prior to 2004, CMT solutions for earthquakes with $M_W < 5.5$ were constrained using long-period ($T > 45$ s) body-wave seismograms, whereas long-period surface-wave ($T > 135$ s, "mantle wave") seismograms were included for larger earthquakes [*Dziewonski et al.*, 1981; *Dziewonski and Woodhouse*, 1983]. Global phase-velocity maps [*Ekström et al.*, 1997] have allowed intermediate-period ($35 < T < 150$ s) surface-wave data to be incorporated in source-parameter inversions for shallow and intermediate-depth $M_W < 7.5$ earthquakes since 2004 [*Arvidsson and Ekström*, 1998; *Ekström et al.*, 2012]. Because intermediate-period surface waves are the largest seismic phases in long-period seismograms for shallow earthquakes, their use in CMT inversions has allowed smaller-magnitude earthquakes to be analyzed by the Global CMT Project. The inclusion of surface waves also improves the quality of GCMT solutions in general since the number of waveforms available for analysis is greatly increased.

[17] Because most GCMT solutions were calculated without intermediate-period surface-wave data, we recalculate CMT solutions for vertical-CLVD earthquakes located near recently active volcanoes. Intermediate-period surface waves have different frequency contents and leave the source at different angles than body waves, and including these data allows us to obtain more robust source parameters. We require target earthquakes from the GCMT catalog to have $|\varepsilon| > 0.20$ and dominant pressure or tension axes plunging more than 50°. We use a value of 50° for the plunge here because we expect that the recalculated CMT solutions for some earthquakes will have dominant pressure or tension axes that plunge more steeply, meeting our final criterion of 60° for selection as vertical-CLVD earthquakes. We restrict our search to those earthquakes with centroid depths less than 50 km that are also located within a 100 km radius of a recently active volcano. Focal mechanisms for the vertical-T earthquakes near Bárdarbunga were recalculated by *Nettles and Ekström* [1998] using methodology similar to that employed here, and we do not include those earthquakes as target events in our study. A total of 134 target earthquakes meet our criteria. We also identify as a target earthquake an M_W 5.8 vertical-T earthquake that occurred on 17 February 2009 in the Kermadec Islands. Although this earthquake did not occur within 100 km of a recently active volcano, it may be associated with volcanic activity at Curtis Island, a remote volcano for which the time of last eruption is unknown [*Smithsonian Institution*, 2009].

2.1.2. The Surface Wave Catalog (1991–2009)

[18] Additional target earthquakes are identified from the Global CMT Project's catalog of surface-wave event locations. The Surface Wave catalog includes most shallow $M > 4.8$ earthquakes reported by global seismicity catalogs,

such as the bulletins of the International Seismological Centre (ISC) and the USGS NEIC, for which event detection is based on the arrival times of high-frequency body-wave phases. The Surface Wave catalog also contains information about other earthquakes that are missing from the ISC and NEIC catalogs due to their small body-wave magnitudes or unusual source properties [*Ekström*, 2006]. Focal mechanisms have so far been calculated for only a small number of earthquakes from the Surface Wave catalog that are not reported in the ISC or NEIC catalogs.

[19] We limit our scope to two categories of earthquakes from the Surface Wave catalog. Category 1 events are earthquakes that are reported in the ISC catalog, but which have surface-wave magnitudes, M_{SW} [*Ekström*, 2006], that are at least one magnitude unit larger than the m_b estimates provided by the ISC. Seventy-four Category 1 earthquakes have surface-wave detections with Quality C or better [*Ekström*, 2006] and initial locations within 100 km of a recently active volcano. Excluding three earthquakes that have non-vertical-CLVD solutions in the GCMT catalog, we identify 71 target earthquakes between 1991 and 2009.

[20] We note that one earthquake, which took place on 26 May 2009 in the Fiji Islands, is a target earthquake in both the GCMT and Surface Wave catalogs. This Category 1 earthquake is especially unusual because it is listed as an m_b 4.5 earthquake with a hypocentral depth of 100 km in the weekly listing of the NEIC's Preliminary Determination of Epicenters (PDEW), while in the GCMT catalog, it is listed as an M_W 5.5 earthquake with a centroid depth fixed to 12 km. With the exception of the May 2009 event, no focal mechanisms are available for the target earthquakes in Category 1.

[21] The second category of earthquakes that we investigate from the Surface Wave catalog are "new" earthquakes that are missing from the ISC and NEIC bulletins, but which were detected and located using intermediate-period surface waves and the method of *Ekström* [2006]. We restrict our search to newly detected earthquakes from 1991 to 2009 that have surface-wave detections with Quality C or better [*Ekström*, 2006] and initial locations within 100 km of a recently active volcano. The vertical-P earthquakes near Nyiragongo from *Shuler and Ekström* [2009] are examples of Category 2 events. Excluding those five events, which have focal mechanisms that were recalculated using methodology similar to that employed here, we identify 190 target earthquakes. No focal mechanisms are available for target earthquakes from Category 2.

2.2. Centroid-Moment-Tensor Solutions

[22] For each of our target earthquakes, we collect three-component long-period and very-long-period seismic data from global and regional networks archived by the Incorporated Research Institutions for Seismology Data Management Center (IRIS DMC). The data sources vary depending on the year, but include stations from the following networks: the Modified High Gain Long Period Observatory (AS), the Black Forest Observatory (BF), the China Digital Seismic Network (CD), the Canadian National Seismic Network (CN), the Czech Seismic Network (CZ), the Digital World-Wide Standardized Seismograph Network (DW), GEOSCOPE (G), GEOFON (GE), the High-Gain Long-Period Network (HG), MEDNET (MN), the Singapore Seismological Network (MS), the Regional Seismic Test Network (RS), the Seismic Research Observatory (SR), TERRAscope (TS), and the IRIS-USGS Global Seismographic Network (GSN), which is a cooperative partnership between the following networks: the IRIS/IDA network (II), the IRIS/USGS Network (IU), the IRIS China Digital Seismic Network (IC), the Global Telemetered Southern Hemisphere Network (GT), and the CariUSGS Caribbean Network (CU). For target earthquakes from the GCMT catalog, the new data sets are typically more complete than those used for the original analysis.

[23] We calculate centroid moment tensors, locations, and times for each target earthquake generally following the standard GCMT approach [*Dziewonski et al*., 1981; *Dziewonski and Woodhouse*, 1983; *Arvidsson and Ekström*, 1998; *Ekström et al*., 2005] and specifically the methods employed since 2004 [*Ekström et al*., 2012]. We manually select and edit seismograms from three frequency bands and time windows. CMT solutions for events with $M_W < 5.5$ are calculated using body-wave data filtered from 40 to 150 s and surface-wave data filtered from 50 to 150 s, while solutions for larger earthquakes also include mantle-wave data filtered from 125 to 350 s. For the smallest earthquakes, we filter the surface-wave data from 40 to 100 s or 35 to 75 s on a case-by-case basis to increase the signal-to-noise ratio. The CMT inversions are based on data from 14 to 163 stations, depending on the year and magnitude of individual target earthquakes. As in the GCMT catalog, we constrain the sum of the diagonal elements of the moment tensor to equal zero ($M_{rr} + M_{\theta\theta} + M_{\phi\phi} = 0$).

[24] We assess the quality of each CMT solution and only report solutions that meet the Global CMT Project's quality standards. In particular, we reject unstable solutions, solutions based on a small number of waveforms and solutions with high residual misfit. We classify earthquakes as "vertical-CLVD" if their moment tensors have 40% or more non-double-couple component and dominant tension or pressure axes that plunge more steeply than 60° (Figure 1). Because we are concerned with vertical-CLVD earthquakes associated with volcanic processes, we restrict our discussion to those events with centroid depths shallower than 25 km.

[25] In this study, we define vertical-CLVD earthquakes based on the properties of the deviatoric moment tensor. However, we recognize that some earthquakes in volcanic areas may have non-zero isotropic components caused by net volume changes. For shallow earthquakes, the isotropic and pure vertical-CLVD components of the moment tensor cannot be independently resolved using long-period seismic data [*Kawakatsu*, 1996]. The presence of Love-wave energy in many of the seismograms we model reduces this tradeoff. However, some earthquakes we identify as having deviatoric vertical-CLVD focal mechanisms may correspond to underlying source processes with dominant isotropic components rather than dominant vertical-CLVD components [*Strelitz*, 1989; *Frohlich*, 1990b]. In our companion paper (Shuler et al., submitted manuscript, 2012), we quantify the tradeoff between the isotropic and pure vertical-CLVD components of the moment tensor for our data set in order to evaluate several potential physical mechanisms for producing earthquakes with deviatoric vertical-CLVD focal mechanisms. These details do not impact our assessment in the current study of the link between the anomalous earthquakes and volcanic unrest.

2.3. Teleseismic Body-Wave Modeling

[26] The vertical-CLVD earthquakes that we identify near active volcanoes are shallow and their depths cannot be determined accurately using the long-period seismic data required for standard GCMT analysis. To confirm that the vertical-CLVD earthquakes have shallow depths consistent with volcanic deformation processes, we attempt to model the broadband teleseismic body waves for earthquakes with magnitudes $M_W \geq 5.0$. For consistency, we attempt the same analysis for vertical-CLVD earthquakes from both the GCMT and Surface Wave catalogs, although we expect lower quality body-wave data for earthquakes from the Surface Wave catalog that were not detected using high-frequency body-wave data.

[27] We follow the method of *Ekström* [1989] and invert teleseismic *P* and *SH* waveforms for focal mechanism, focal depth, and moment-rate function. For this analysis, we collect broadband seismic records from the IRIS DMC and deconvolve the instrument response to obtain displacement records filtered from 1 to 100 s period. We model *P* waveforms using data from the vertical component. We model *SH* waveforms using data from horizontal components rotated to the transverse direction at each station. Following the method of *Harvey and Choy* [1982], broadband records for the oldest earthquakes are constructed from digital long- and short-period seismograms, as in *Ekström* [1989]. Synthetic seismograms are calculated using ray theory and the Preliminary Reference Earth Model (PREM) [*Dziewonski and Anderson*, 1981]. Reflections and conversions near the source are modeled using a layer-matrix method for a regional velocity model. For a small number of subaerial volcanoes, we construct the regional velocity models using the local crustal structure from CRUST2.0 [*Bassin et al*., 2000]. However, for those earthquakes near island arc or submarine volcanoes, we use the CRUST2.0 model for a Japanese island arc (J1) and adjust the thickness of the water layer to match the summit elevation of the nearest volcano. We include the CMT estimate of the point-source moment tensor as a soft constraint in the inversions to ensure that focal mechanisms calculated from the broadband data are compatible with the long-period seismic data used in the CMT analysis.

3. Results

[28] Of the 395 target earthquakes investigated, we obtain robust CMT solutions for 313 earthquakes. Focal mechanisms are plotted in Figure 3 and source-parameter information is available in the auxiliary material[1] as well as on our website (www.globalcmt.org). We report updated CMT solutions for 124 earthquakes from the GCMT catalog (Tables S1 and S2) and new CMT solutions for 190 earthquakes from the Surface Wave catalog, including 59 Category 1 earthquakes (Tables S3 and S4) and 131 Category 2 earthquakes (Tables S5 and S6). We note that the 26 May 2009 earthquake is reported in both the GCMT and Surface Wave catalogs.

[29] From this group of 313 earthquakes, we identify 86 shallow vertical-CLVD earthquakes located near recently active volcanoes. We are able to model teleseismic body waves from 18 of these events. Along with the 15 vertical-CLVD earthquakes already documented at Bárdarbunga [*Nettles and Ekström*, 1998] and Nyiragongo volcanoes [*Shuler and Ekström*, 2009], this study increases the number of well-documented, moderate-sized shallow vertical-CLVD earthquakes known to occur near volcanic centers to 101.

3.1. All Target Earthquakes

[30] The recalculated CMT solutions for target events from the GCMT catalog are based on both body and surface-wave data that were manually selected and edited. Because the new solutions described in Tables S1 and S2 were calculated using additional data and updated methodology, they are more robust than those reported in the standard GCMT catalog. The recalculated CMT solutions are the preferred solutions for the target earthquakes. Compared to the original GCMT solutions, the recalculated moment tensors changed by ~0.1 magnitude units and the centroid locations moved ~30 km on average. As expected, differences between the original and recalculated CMT solutions are smaller for earthquakes that occurred after 2004, when the Global CMT Project began to use surface-wave data routinely.

[31] For most target earthquakes from the GCMT catalog, we find that the addition of surface-wave data reduces the size of the non-double-couple component, resulting in new moment tensors that are approximately double couple. Recalculated moment tensors for most vertical-T and vertical-P earthquakes are typical of reverse- and normal-faulting earthquakes. In many cases, the new focal mechanisms are consistent with those reported in the GCMT catalog for other nearby earthquakes. Only 26 of the earthquakes considered, 18 vertical-T and 8 vertical-P earthquakes, have vertical-CLVD moment tensors and centroid depths less than 25 km after the addition of surface-wave data. Included in this data set are the four vertical-T earthquakes identified by *Ekström* [1994] that did not occur near Bárdarbunga. In Figure 4, we illustrate how the addition of surface-wave data affects the CMT solutions for one earthquake that became more double couple and one that remained vertical-CLVD.

[32] Target earthquakes from the Surface Wave catalog have a wide variety of focal mechanisms, reflecting the diversity of tectonic settings located within a 100 km radius of recently active volcanoes. In Tables S3–S6, we provide CMT solutions for these earthquakes. For both Category 1 and Category 2 events, we find that moment tensors for most of the target earthquakes are close to double couple. The most commonly observed earthquake types are strike-slip and normal-faulting earthquakes along the ridge-transform systems near Tonga, Vanuatu, Samoa, Fiji, and the Mariana Islands. Shallow strike-slip earthquakes in the southern oceans are particularly difficult to detect using traditional methods due to their nearly nodal teleseismic *P*-wave radiation patterns, their remoteness from seismic stations, and the presence of strong microseismic noise [*Rouland et al*., 1992; *Shearer*, 1994], and some go unreported in standard global seismicity catalogs.

[33] Of the 190 target earthquakes investigated from the Surface Wave catalog, 61 have vertical-CLVD moment tensors. Including the 26 May 2009 event, which is also reported in the GCMT catalog, eight earthquakes have vertical-T moment tensors and 53 have vertical-P moment

[1]Auxiliary materials are available in the HTML. doi:10.1029/2012GC009721.

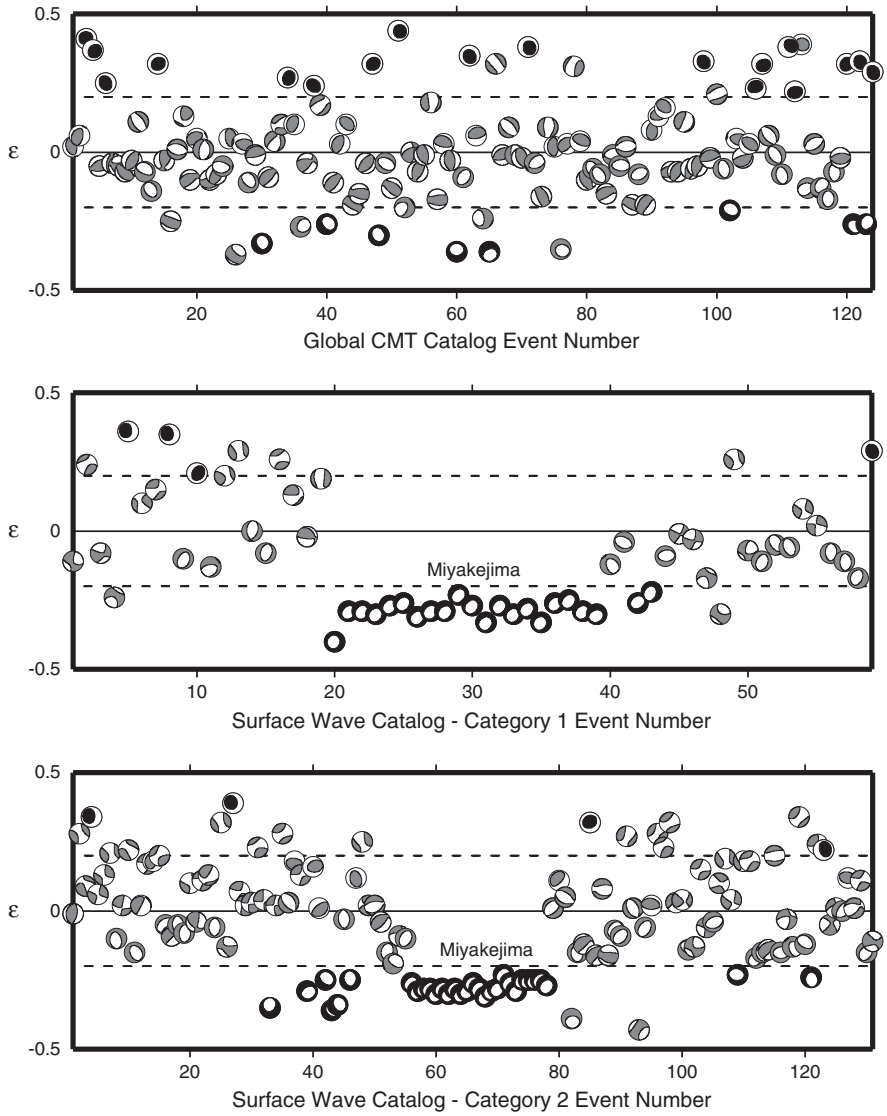

Figure 3. Focal mechanisms for all of the target earthquakes for which we were able to obtain robust CMT solutions, plotted against their ε values. Shallow vertical-CLVD earthquakes are plotted in black, and the dashed lines indicate $\varepsilon = \pm 0.20$. The top panel shows focal mechanisms for 124 earthquakes from the Global CMT catalog after reanalysis. The middle panel shows focal mechanisms for 59 Category 1 earthquakes from the Surface Wave catalog, and the bottom panel shows focal mechanisms for 131 Category 2 earthquakes from the Surface Wave catalog. The event numbers correspond to the event numbers reported in Tables S1–S6. The 43 vertical-P earthquakes associated with the caldera collapse of Miyakejima in 2000 are indicated in the middle and bottom panels.

tensors. Forty-three of the vertical-P earthquakes are associated with a single volcano, Miyakejima.

[34] We were not able to calculate CMT solutions for several Category 2 target earthquakes that are spatially and temporally associated with explosive eruptions that produced large-scale pyroclastic density currents. These events include the sector collapse and lateral blast event at Soufrière Hills volcano in the West Indies on 26 December 1997 [*Calder et al*., 2002; *Druitt et al*., 2002; *Ritchie et al*., 2002; *Sparks et al*., 2002; *Voight et al*., 2002; *Woods et al*., 2002; *Young et al*., 2002], and several pre-climactic eruptions at Pinatubo volcano in the Philippines on 14 and 15 June 1991 [*Harlow et al*., 1996; *Hoblitt et al*., 1996; *Lynch and Stephens*, 1996; *Power et al*., 1996; *Wolfe and Hoblitt*, 1996]. If the seismic signals that we observe are produced by gravity-driven flows, it may be more appropriate to model these events using time-varying forces.

3.2. Vertical-CLVD Earthquakes

[35] In total, we have identified 101 shallow vertical-CLVD earthquakes with centroid locations near recently active volcanoes. In Figures 5 and 6, we show the locations and focal mechanisms of vertical-CLVD earthquakes from the GCMT and Surface Wave catalogs. Figure 7 shows a map of the vertical-P earthquakes associated with Miyakejima volcano. In these three maps, red focal mechanisms denote earthquakes that are associated with volcanic unrest at a volcano within ~60 km (section 4). For each of the

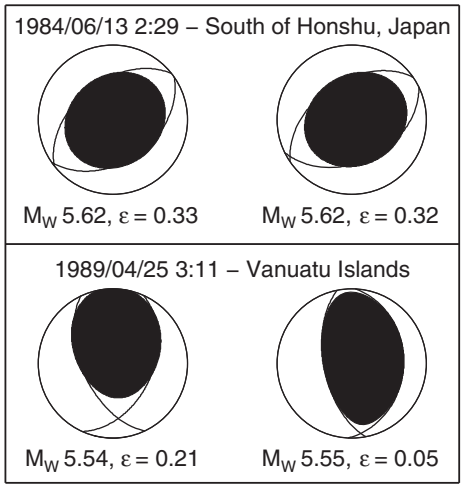

Figure 4. A comparison between the original CMT solutions (left), calculated using body waves, and new CMT solutions (right), calculated in this study using body and surface waves, for two earthquakes. The moment magnitude and ε value associated with each CMT solution are indicated below the focal mechanisms. Thin solid lines show the double-couple part of the focal mechanisms. The top panel is for the Tori Shima earthquake. The original solution was calculated using body-wave data from 15 stations, and the new solution was calculated using body-wave data from 20 stations, mantle-wave data from six stations, and surface-wave data from 22 stations. The bottom panel is for an earthquake in the Vanuatu Islands. The original solution was calculated using body-wave data from 22 stations, and the new solution was calculated using body-wave data from 15 stations, mantle-wave data from 12 stations, and surface-wave data from 27 stations. The Tori Shima earthquake remained vertical-CLVD after the addition of surface-wave data whereas the Vanuatu earthquake became approximately double couple.

86 vertical-CLVD earthquakes analyzed in this study, we provide in Table 1 a summary of source parameters including centroid times and locations, m_b values from the NEIC, as well as M_W values, ε values, and plunges of the dominant principal axes derived from the CMT solutions. We do not report the centroid depths of vertical-CLVD earthquakes in Table 1 because they were all fixed to 12 km during the inversion process, as is standard for very shallow earthquakes.

[36] In Tables S7 and S8 in the auxiliary material, we provide detailed information about the CMT solutions for vertical-CLVD earthquakes, including estimates of the standard errors for the source parameters. The standard errors associated with the latitude and longitude components are ~3 km on average, although due to uneven station distributions, the presence of noise and remaining unmodeled structural heterogeneity [e.g., *Nakanishi and Kanamori*, 1982; *Dziewonski and Woodhouse*, 1983; *Dziewonski et al*., 1983; *Dziewonski et al*., 1984; *Smith and Ekström*, 1997; *Hjörleifsdóttir and Ekström*, 2010], the actual uncertainties are likely larger. For example, the centroid locations for vertical-CLVD earthquakes linked to specific episodes of volcanic unrest are sometimes tens of kilometers from their source volcanoes.

[37] We assess the quality of each CMT solution based on the station coverage, the variance reduction, and the percentage of available waveforms used in the inversion (Table 1). A-quality CMT solutions have variance reductions of 50% or more and are calculated using data from 75% or more of the available stations. CMT solutions that have variance reductions of 40–50%, azimuthal gaps greater than 90°, and those that are calculated using data from 50% to 75% of the available stations are assigned B quality. We assign the two earthquakes that have fixed centroid locations to be C quality, in addition to those solutions that are calculated using less than 50% of the available stations, or those that have variance reductions less than 40%. We find that 47 earthquakes have A-quality solutions, 26 have B-quality solutions, and 13 have C-quality solutions. However, all of the solutions meet the quality standards of the Global CMT Project. Our confidence in the significance of the vertical-CLVD component is a function of both the CMT solution quality and the magnitude of the non-double-couple component.

[38] To confirm that the vertical-CLVD earthquakes have shallow focal depths, we attempted to model the broadband teleseismic body waves for vertical-CLVD earthquakes with magnitudes $M_W \geq 5.0$. However, we were only able to model 18 earthquakes, all from the GCMT catalog. Teleseismic body waves for earthquakes in the Surface Wave catalog are of lower amplitude than the background noise across the frequency band we examine, and we were not able to model any body waves for these events.

[39] Earthquakes in this magnitude range ($5.0 \leq M_W \leq 6.0$) typically show clear, impulsive direct arrivals and surface reflections. In contrast, we find that the body waves for vertical-CLVD earthquakes are dominated by low-frequency energy. Figure 8 shows an example body-wave solution for the M_W 5.7 vertical-T earthquake that occurred south of Honshu on 4 September 1996. The fit to the data illustrated in Figure 8 is typical for the events we analyze. We find that focal-depth estimates depend on the weight of the soft constraint of the long-period moment tensors from the CMT inversions, and there is a tradeoff between focal depth and source duration. Despite the uncertainties associated with modeling body waves for earthquakes depleted in high-frequency energy, the character of the waveforms for all 18 earthquakes is consistent with focal depths in the top 10 km of the crust.

4. Links to Volcanic Activity

[40] Our target earthquakes were selected because they occurred near active volcanoes, but there were no restrictions on volcano type or location. In our data set of shallow vertical-CLVD earthquakes, we observe events near active volcanoes in a wide variety of geographical locations and tectonic settings. In Table 2, we list the three closest volcanoes to each vertical-CLVD earthquake. We report the distances from the centroid location of each earthquake to the three closest volcanoes using the latitude and longitude coordinates provided by the GVP [*Siebert and Simkin*, 2002]. The length scales of volcanic systems, which range from a few hundred meters to tens of kilometers, should be considered when interpreting these distances. We also report the volcano type, or morphology, of the closest volcanoes and indicate

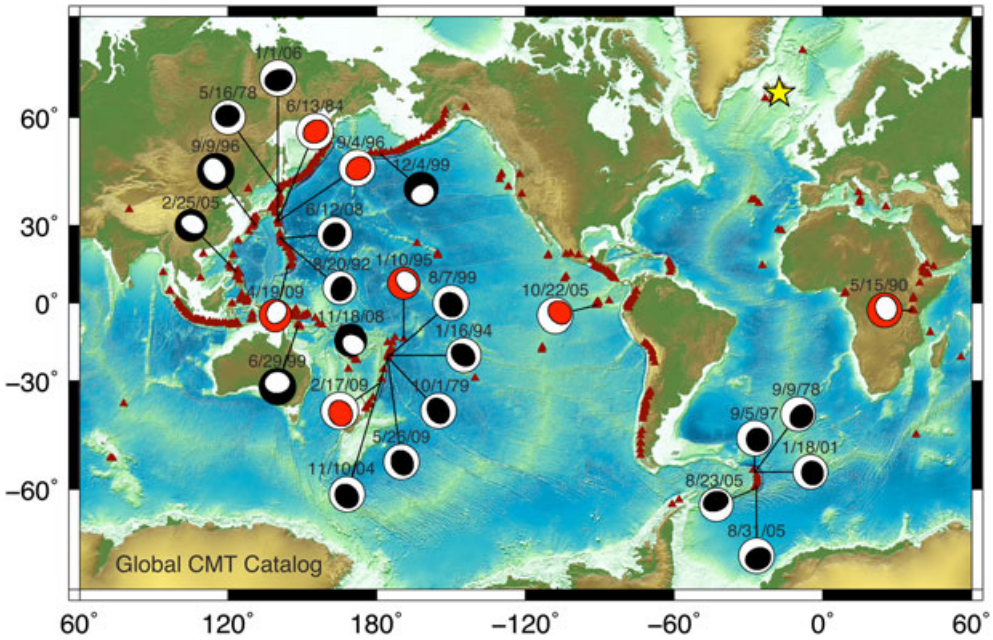

Figure 5. Map showing focal mechanisms for the 26 shallow vertical-CLVD earthquakes identified from the Global CMT catalog. Red focal mechanisms indicate that the earthquakes are associated with a documented episode of volcanic unrest at a nearby volcano (see text for details). The dates of the earthquakes are listed above the focal mechanisms. Maroon triangles indicate the locations of the 429 recently active volcanoes. A yellow star indicates the location of Bárdarbunga volcano, where 10 vertical-T earthquakes occurred between 1976 and 1996 [*Nettles and Ekström*, 1998]. Bathymetry and topography are from the ETOPO1 data set.

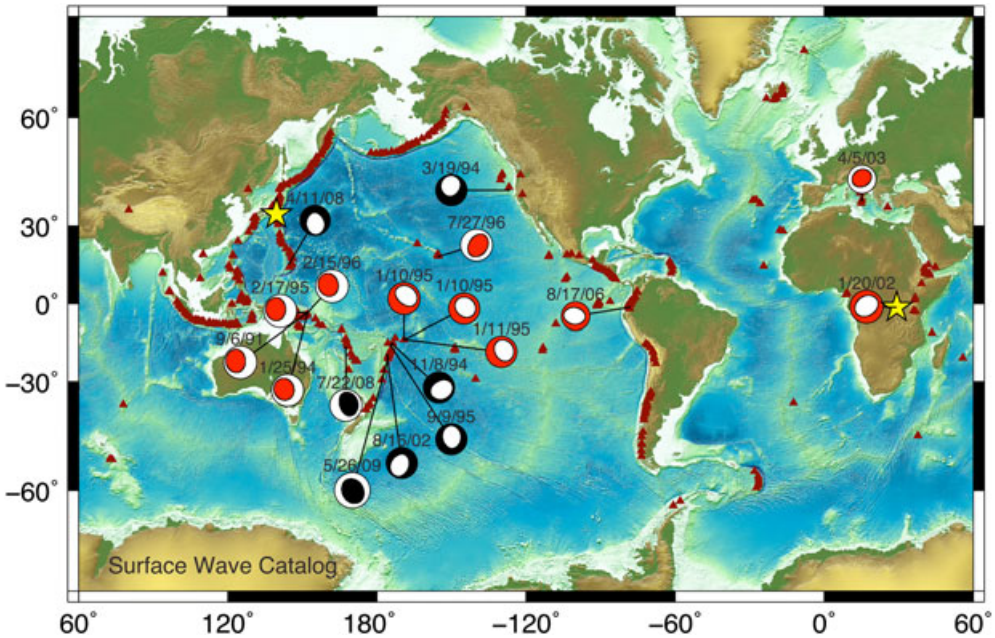

Figure 6. Map showing focal mechanisms for 18 shallow vertical-CLVD earthquakes from CMT analysis of events in the Surface Wave catalog. The vertical-T earthquake on 26 May 2009 is repeated from Figure 5. Red focal mechanisms indicate that the earthquakes are associated with a documented episode of volcanic unrest at a nearby volcano (see text for details). The dates of the earthquakes are listed above the focal mechanisms. Maroon triangles indicate the locations of the 429 recently active volcanoes. Yellow stars indicate the locations of Miyakejima volcano, where another 43 vertical-P earthquakes occurred in 2000 (Figure 7), and Nyiragongo, where five vertical-P earthquakes occurred between 2002 and 2005 [*Shuler and Ekström*, 2009]. Bathymetry and topography are from the ETOPO1 data set.

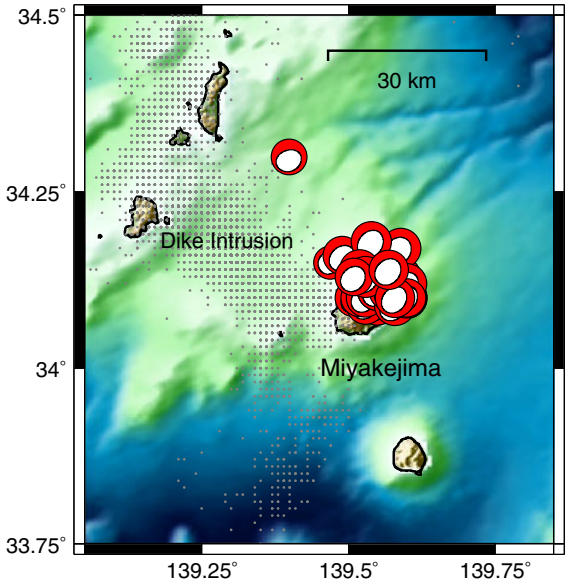

Figure 7. Map showing focal mechanisms for the 43 vertical-P earthquakes associated with the caldera collapse of Miyakejima volcano between 7 July and 18 August 2000. Focal mechanisms are plotted at their centroid locations. The earthquake with the centroid location that is farthest away from Miyakejima occurred on 18 August 2000 at 9:09 UTC. Grey dots show the locations of earthquakes associated with the dike intrusion that began at Miyakejima on 26 June 2000. Epicenters for earthquakes from June to December 2000 are provided by the Japan Meteorological Agency. The grid-like pattern is due to the precision with which the epicenters are reported. Topography is from the Shuttle Radar Topography Mission (SRTM). Bathymetry is from the Japan Oceanographic Data Center J-EGG500 data set.

whether the earthquakes occurred during documented episodes of volcanic unrest. Most vertical-CLVD earthquakes are located within ~30 km of arc volcanoes in subduction zones in the Pacific, Indian, and Southern Oceans and the Mediterranean Sea. However, vertical-CLVD earthquakes also occur in the East African Rift, along a mid-ocean ridge segment in the northeastern Pacific Ocean, and near hot spot volcanoes in Hawaii, the Galápagos Islands, and Samoa Islands. This result suggests that many types of volcanoes are capable of generating vertical-CLVD earthquakes, and strengthens the link between volcanoes and these anomalous earthquakes.

[41] We wish to assess not only the spatial but also the temporal relationships between the vertical-CLVD earthquakes and volcanism. To assess the likelihood that the earthquakes result, directly or indirectly, from active magma transport in the crust, we evaluate whether each vertical-CLVD earthquake in our data set is associated with known eruptive or other volcanic activity. Below, we summarize the location of each vertical-CLVD earthquake and its temporal relationship to volcanic unrest at nearby volcanoes. First, in chronological order by the first earthquake at each volcano, we discuss the 61 vertical-CLVD earthquakes that are spatially and temporally associated with volcanic unrest, using eruption reports from the literature. We then summarize the locations of the remaining 24 vertical-CLVD earthquakes by geographic location. Unless otherwise indicated, the CMT solutions discussed are A quality and the information about specific volcanoes is from the GVP [*Siebert and Simkin*, 2002].

4.1. Smith Rock

[42] Three M_W 5.6–5.7 vertical-T earthquakes in the Izu-Bonin volcanic arc have centroid locations that are ~10–20 km from Smith Rock, a basaltic pinnacle that forms the southern flank of a 20 km-wide seamount with an 8–9 km wide submarine caldera. The first earthquake is the 13 June 1984 Tori Shima earthquake discussed in section 1. The Tori Shima earthquake produced an $M_t = 7.3$ tsunami [*Abe*, 1988; *Satake and Kanamori*, 1991] and was followed within hours by earthquakes with *T*-wave trains, which are characteristic of submarine volcanic activity [*Talandier and Okal*, 1987]. The second and third earthquakes occurred on 4 September 1996 and 1 January 2006. Similar to the Tori Shima earthquake, the 1996 earthquake produced an $M_t = 7.5$ tsunami and was followed by a swarm of low-frequency earthquakes that produced *T* waves [*Sugioka et al.*, 2000], again suggesting volcanic activity. Both the 1984 and 1996 earthquakes initiate episodes of volcanic unrest at Smith Rock, which suggests that the vertical-T earthquakes may be associated with magma ascent processes. The 2006 earthquake, which has the smallest non-double-couple component, is not linked to any known volcanic unrest.

4.2. Ol Doinyo Lengai

[43] An M_W 5.4 vertical-P earthquake with a B-quality CMT solution took place in Tanzania on 15 May 1990. The centroid location is ~25 km from Ol Doinyo Lengai, one of the most active volcanoes in the East African Rift. Ol Doinyo Lengai is a stratovolcano and the only known active volcano to erupt natrocarbonatite, a silica-poor, low-temperature, and low-viscosity lava [*Oppenheimer*, 1998]. Before erupting explosively in 2007, Ol Doinyo Lengai erupted effusively for nearly 25 years, producing lava flows and spatter cones that were confined to the summit crater. Effusive activity was observed both before and after the 15 May earthquake, during overflights on 2 May and 9 July 1990 [*Smithsonian Institution*, 1990a, 1990b], which suggests that the vertical-P earthquake is related to this prolonged effusive eruption.

4.3. Rabaul

[44] Four M_W 5.0 vertical-T earthquakes took place north of New Britain in Papua New Guinea between 1991 and 1996. These earthquakes occurred on 6 September 1991, 25 January 1994, 17 February 1995, and 15 February 1996. The vertical-CLVD earthquakes have A or B-quality CMT solutions and focal mechanisms that are remarkably similar between events. The centroid locations are tightly clustered near the tip of the Gazelle Peninsula, ~35 km north of Tavui, a 10-by-12 km submarine caldera, and ~50 km north of Rabaul, an active pyroclastic shield volcano with a nested 9-by-14 km caldera complex surrounded by several small volcanic cones. The last eruption of Tavui occurred approximately 7000 years ago [*Nairn et al.*, 1995; *Wood et al.*, 1995], although recent seismic tomography studies indicate the presence of a low-velocity zone beneath the

Table 1. Source Parameters for 86 Shallow Vertical-CLVD Earthquakes Located Near Recently Active Volcanoes[a]

No.	Source Catalog	Date			Time			Centroid Latitude	Centroid Longitude	Geographical Location	m_b	M_W	ε	Plunge of P/T Axis	CMT Quality
		Y	M	D	h	m	s								
1	GCMT	1978	5	16	7	35	49.1	40.99	141.44	Hokkaido, Japan	5.7	5.3	0.41	82	A
2	GCMT	1978	9	9	6	1	7.6	−56.34	−27.31	South Sandwich Islands Region	5.4	5.4	0.37	68	B
3	GCMT	1979	10	1	12	23	51.2	−21.29	−175.66	Tonga Islands	5.1	5.5	0.25	88	B
4	GCMT	1984	6	13	2	29	29.8	31.57	139.97	South of Honshu, Japan	5.6	5.6	0.32	85	A
5	GCMT	1990	5	15	15	21	31.1	−2.96	35.80	Tanzania	5.5	5.4	−0.33	77	B
6	SW-2	1991	9	6	5	40	54.6	−3.85	152.03	New Ireland, Papua New Guinea		5.0	0.34	63	A
7	GCMT	1992	8	20	18	31	39.9	25.43	141.13	Volcano Islands, Japan		5.2	0.27	80	A
8	GCMT	1994	1	16	10	18	41.5	−20.62	−175.20	Tonga Islands	4.8	5.3	0.24	87	A
9	SW-2	1994	1	25	23	15	1.9	−3.82	152.05	New Ireland, Papua New Guinea		5.0	0.39	70	B
10	SW-2	1994	3	19	21	49	42.9	41.67	−127.06	Off Coast of Oregon		4.7	−0.35	62	B
11	SW-2	1994	11	8	13	7	56.8	−15.91	−173.97	Tonga Islands		4.8	−0.29	69	B
12	GCMT	1995	1	10	13	43	37.3	−14.22	−169.06	Samoa Islands		4.9	−0.26	70	C
13	SW-2	1995	1	10	17	44	0.1	−14.24	−169.03	Samoa Islands		4.9	−0.25	68	B
14	SW-2	1995	1	10	23	49	26.3	−14.25	−168.97	Samoa Islands		4.8	−0.36	79	B
15	SW-2	1995	1	11	18	16	5.9	−14.18	−169.00	Samoa Islands		4.8	−0.34	71	B
16	SW-1	1995	2	17	17	45	42.7	−3.85	152.10	New Ireland, Papua New Guinea	3.5	5.0	0.36	64	B
17	SW-2	1995	9	9	15	53	17.4	−16.59	−174.38	Tonga Islands		4.8	−0.25	75	C
18	SW-1	1996	2	15	1	11	43.0	−3.85	152.03	New Ireland, Papua New Guinea	3.7	5.0	0.35	67	B
19	SW-1	1996	7	27	13	6	38.6	18.77	−155.18	Hawaii		4.9	0.21	79	C
20	GCMT	1996	9	4	18	16	7.7	31.51	139.99	South of Honshu, Japan	5.4	5.7	0.32	82	A
21	GCMT	1996	9	9	4	34	21.9	30.44	130.95	Kyushu, Japan	5.5	5.7	−0.30	83	A
22	GCMT	1997	9	5	3	23	17.0	−56.41	−27.47	South Sandwich Islands Region	5.2	5.4	0.44	73	A
23	GCMT	1999	6	29	5	50	9.2	−9.59	147.97	East Papua New Guinea	5.8	5.6	−0.36	69	B
24	GCMT	1999	8	7	6	17	30.5	−21.24	−175.61	Fiji Islands Region	5.0	5.5	0.35	81	A
25	GCMT	1999	12	4	8	46	57.7	51.56	−178.29	Andreanof Islands, Aleutian Islands	5.2	5.1	−0.36	60	B
26	SW-1	2000	7	7	11	22	4.3	34.15	139.47	Near South Coast of Honshu, Japan	3.4	4.4	−0.40	79	C
27	SW-1	2000	7	9	13	40	15.3	34.11	139.56	Near South Coast of Honshu, Japan	2.5	5.2	−0.29	79	B
28	SW-2	2000	7	10	17	11	52.0	34.09	139.55	Near South Coast of Honshu, Japan		5.4	−0.26	80	A
29	SW-1	2000	7	11	15	37	31.5	34.10	139.59	Near South Coast of Honshu, Japan	4.0	5.3	−0.29	80	A
30	SW-1	2000	7	12	4	7	0.0	34.13	139.57	Near South Coast of Honshu, Japan	3.4	5.2	−0.30	79	A
31	SW-1	2000	7	12	18	45	55.6	34.12	139.58	Near South Coast of Honshu, Japan	2.7	5.3	−0.27	79	A
32	SW-1	2000	7	13	17	12	29.8	34.10	139.60	Near South Coast of Honshu, Japan	2.6	5.5	−0.26	79	A
33	SW-1	2000	7	15	14	34	46.4	34.14	139.57	Near South Coast of Honshu, Japan	2.4	5.3	−0.31	79	A
34	SW-2	2000	7	16	1	37	55.0	34.12	139.59	Near South Coast of Honshu, Japan		5.2	−0.29	79	A
35	SW-2	2000	7	16	17	11	51.3	34.12	139.55	Near South Coast of Honshu, Japan		5.2	−0.28	80	C
36	SW-2	2000	7	17	8	26	41.3	34.10	139.58	Near South Coast of Honshu, Japan		5.2	−0.28	79	A
37	SW-2	2000	7	17	21	35	45.4	34.10	139.60	Near South Coast of Honshu, Japan		5.2	−0.30	78	A
38	SW-2	2000	7	18	20	32	29.5	34.13	139.59	Near South Coast of Honshu, Japan		5.4	−0.28	81	A
39	SW-2	2000	7	19	16	15	40.0	34.10	139.51	Near South Coast of Honshu, Japan		5.1	−0.30	80	B
40	SW-1	2000	7	20	8	24	17.4	34.11	139.58	Near South Coast of Honshu, Japan	1.5	5.3	−0.29	78	A
41	SW-1	2000	7	21	0	27	51.4	34.16	139.49	Near South Coast of Honshu, Japan	2.5	5.2	−0.29	77	B
42	SW-2	2000	7	21	15	7	21.3	34.09	139.53	Near South Coast of Honshu, Japan		5.1	−0.28	83	A
43	SW-2	2000	7	22	5	1	23.9	34.14	139.53	Near South Coast of Honshu, Japan		5.2	−0.30	77	A
44	SW-2	2000	7	22	17	20	43.9	34.10	139.52	Near South Coast of Honshu, Japan		5.0	−0.29	83	A
45	SW-1	2000	7	23	16	36	44.5	34.13	139.55	Near South Coast of Honshu, Japan	3.8	5.2	−0.23	80	A
46	SW-2	2000	7	24	5	25	20.0	34.10	139.53	Near South Coast of Honshu, Japan		5.2	−0.26	79	A
47	SW-1	2000	7	24	19	55	37.3	34.11	139.55	Near South Coast of Honshu, Japan	2.3	5.3	−0.27	76	A
48	SW-2	2000	7	25	9	55	32.1	34.09	139.58	Near South Coast of Honshu, Japan		5.1	−0.28	80	A
49	SW-1	2000	7	25	20	10	28.0	34.14	139.55	Near South Coast of Honshu, Japan	1.7	5.2	−0.33	76	A
50	SW-2	2000	7	26	3	57	54.9	34.12	139.56	Near South Coast of Honshu, Japan		5.1	−0.31	79	A
51	SW-2	2000	7	26	13	29	43.8	34.11	139.55	Near South Coast of Honshu, Japan		5.3	−0.29	76	A
52	SW-1	2000	7	27	7	22	50.4	34.13	139.59	Near South Coast of Honshu, Japan	2.9	5.4	−0.27	77	A
53	SW-1	2000	7	28	7	7	39.3	34.10	139.58	Near South Coast of Honshu, Japan	2.8	5.4	−0.30	75	A
54	SW-1	2000	7	29	7	51	38.8	34.12	139.57	Near South Coast of Honshu, Japan	2.7	5.5	−0.28	77	A
55	SW-1	2000	7	30	13	36	33.5	34.17	139.59	Near South Coast of Honshu, Japan	3.2	5.5	−0.33	75	B
56	SW-2	2000	7	31	22	45	0.9	34.18	139.54	Near South Coast of Honshu, Japan		5.4	−0.28	78	B
57	SW-2	2000	8	2	6	15	35.8	34.09	139.58	Near South Coast of Honshu, Japan		5.6	−0.23	80	A
58	SW-1	2000	8	3	19	16	42.1	34.14	139.52	Near South Coast of Honshu, Japan	3.7	5.5	−0.26	78	B
59	SW-2	2000	8	4	16	11	13.6	34.11	139.57	Near South Coast of Honshu, Japan		5.4	−0.26	79	A
60	SW-1	2000	8	6	0	23	22.7	34.13	139.53	Near South Coast of Honshu, Japan	3.4	5.5	−0.25	78	B
61	SW-2	2000	8	8	0	3	29.3	34.13	139.51	Near South Coast of Honshu, Japan		5.1	−0.29	78	A
62	SW-2	2000	8	8	17	11	58.6	34.10	139.60	Near South Coast of Honshu, Japan		5.4	−0.25	80	A
63	SW-2	2000	8	10	22	2	47.4	34.11	139.59	Near South Coast of Honshu, Japan		5.5	−0.25	79	A
64	SW-2	2000	8	13	6	40	21.4	34.12	139.60	Near South Coast of Honshu, Japan		5.5	−0.25	78	A
65	SW-2	2000	8	16	0	7	29.2	34.10	139.60	Near South Coast of Honshu, Japan		5.2	−0.25	80	B
66	SW-2	2000	8	16	15	57	6.7	34.10	139.58	Near South Coast of Honshu, Japan		5.3	−0.27	80	A
67	SW-1	2000	8	17	19	7	44.2	34.14	139.57	Near South Coast of Honshu, Japan	1.9	5.4	−0.29	78	A
68	SW-1	2000	8	18	9	9	16.3	34.30	139.40	Near South Coast of Honshu, Japan	2.4	4.8	−0.30	70	B
69	GCMT	2001	1	18	20	17	17.4	−56.31	−27.43	South Sandwich Islands Region	5.2	5.3	0.38	77	B
70	SW-1	2002	1	20	23	45	31.6	−1.42	29.13	Lake Tanganyika Region	4.1	5.1	−0.26	84	C

Table 1. (continued)

No.	Source Catalog	Date Y	M	D	Time h	m	s	Centroid Latitude	Centroid Longitude	Geographical Location	m_b	M_W	ε	Plunge of P/T Axis	CMT Quality
71	SW-1	2002	8	16	21	30	47.5	−20.28	−175.99	Tonga Islands	3.7	4.7	−0.22	72	C
72	SW-2	2003	4	5	7	13	45.5	38.65	15.19	Sicily, Italy		4.3	0.32	83	C
73	GCMT	2004	11	10	10	35	38.0	−21.26	−175.62	Fiji Islands Region	5.0	5.5	0.33	80	A
74	GCMT	2005	2	25	16	17	1.6	12.77	123.23	Luzon, Philippines	4.9	4.9	−0.21	76	B
75	GCMT	2005	8	23	1	38	20.1	−59.80	−26.68	South Sandwich Islands Region	5.1	5.1	0.23	71	B
76	GCMT	2005	8	31	1	24	54.9	−59.48	−26.86	South Sandwich Islands Region	5.3	5.5	0.32	71	B
77	GCMT	2005	10	22	20	34	47.9	−1.06	−91.31	Galapagos Islands, Ecuador	4.9	5.5	0.38	62	A
78	GCMT	2006	1	1	7	12	8.8	31.60	140.17	Southeast of Honshu, Japan	5.3	5.6	0.22	81	A
79	SW-2	2006	8	17	5	37	21.2	−1.47	−78.44	Ecuador		4.4	−0.23	82	C
80	SW-2	2008	4	11	0	46	13.3	16.09	144.69	Mariana Islands		4.7	−0.24	69	C
81	GCMT	2008	6	12	13	10	14.7	25.53	141.18	Volcano Islands, Japan	5.1	5.3	0.32	86	A
82	SW-2	2008	7	22	8	45	22.4	−17.36	167.52	Vanuatu Islands		4.9	0.22	71	C
83	GCMT	2008	11	18	12	46	3.8	−18.76	169.55	Vanuatu Islands	4.9	5.0	−0.26	65	C
84	GCMT	2009	2	17	3	30	58.8	−30.54	−178.58	Kermadec Islands, New Zealand	5.4	5.8	0.33	78	A
85	GCMT	2009	4	19	8	54	52.8	14.66	144.23	Mariana Islands	4.7	4.9	−0.26	72	C
86	GCMT/SW-1	2009	5	26	0	49	42.9	−21.24	−175.62	Fiji Islands Region	4.5	5.5	0.29	85	A

[a]Source Catalogs are Global CMT catalog (GCMT) or Surface Wave Catalog (SW). SW-1 denotes events reported in the ISC or NEIC catalogs where $M_{SW} - m_b \geq 1.0$. SW-2 denotes earthquakes that were newly detected using surface waves *Ekström* [2006]. The date, time, centroid longitude and latitude, and values of M_W, ε, and the plunge of the dominant *P* or *T* axes are derived from our CMT solutions. We follow the GCMT convention for calculating M_W; scalar moment is defined by the equation $M_0 = 0.5(\lambda_1 - \lambda_3)$, where λ_1 and λ_3 are the maximum and minimum eigenvalues of the deviatoric moment tensor. The m_b values are from the ISC or NEIC catalogs. See text for explanation of CMT quality. Note that all centroid depths from the CMT solutions were fixed to 12 km.

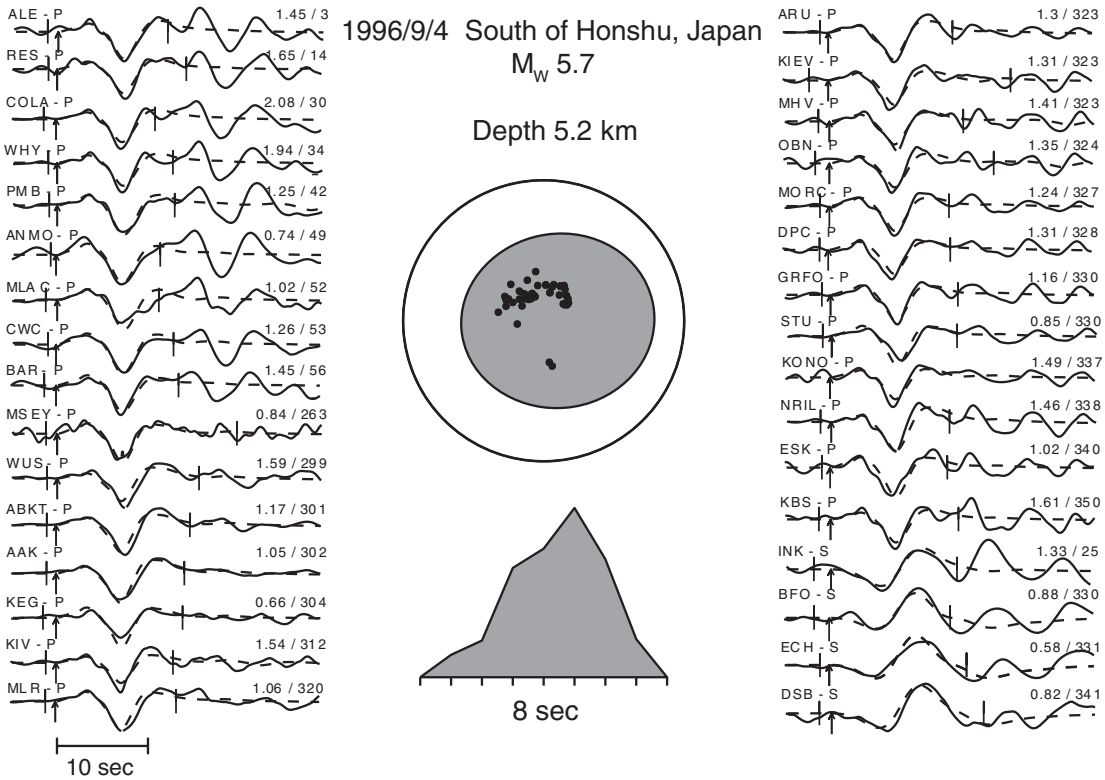

Figure 8. Focal-depth analysis for the M_W 5.7 earthquake that occurred on 4 September 1996 near Smith Rock volcano in the Izu-Bonin volcanic arc. Solid lines show selected, typical broadband teleseismic *P* and *SH* waveforms modeled for this event; dashed lines are synthetic seismograms. Brackets across the waveforms show the portions of the seismograms that were used in the inversion, and arrows indicate the picked first arrivals. The station name, data type, maximum amplitude (in microns), and azimuth from source to station (in degrees) are printed above each waveform. Waveforms are ordered by data type and azimuth. The focal mechanism and moment-rate function determined in the body-wave inversion are plotted in the center of the figure. Black dots on the focal mechanism show where all modeled waveforms exited the focal sphere. The estimated focal depth of the earthquake is ~5.2 km.

Table 2. Volcanoes Located Near Shallow Vertical-CLVD Earthquakes[a]

Three Nearest Volcanoes Within 100 km of Shallow Vertical-CLVD Earthquakes												
No.	Volcano 1	D1 (km)	Type	Unrest?	Volcano 2	D2 (km)	Type	Unrest?	Volcano 3	D3 (km)	Type	Unrest?
1	*Osore-yama*	42	Stratovolcano	No	*Hakkoda Group*	60	Stratovolcanoes	No	*Towada*	73	Caldera	No
2	*Zavodovski*	17	Stratovolcano	No	*Hodson*	41	Stratovolcano	No	*Leskov Island*	62	Stratovolcano	No
3	Unnamed (0403-01)	10	Submarine Volcano	No	*Unnamed (0403-011)*	18	Submarine Volcano	No	Unnamed (0403-03)	51	Submarine Volcano	No
*4	Smith Rock	16	Submarine Volcano	Yes	Bayonnaise Rocks	35	Submarine Volcano	No	*Myojin Knoll*	60	Submarine Volcano	No
*5	Ol Doinyo Lengai	25	Stratovolcano	Yes								
*6	*Tavui*	35	Caldera	No	Rabaul	50	Pyroclastic Shield	Yes				
7	Kita-Iwo-jima	15	Stratovolcano	No	Kaitoku Seamount	77	Submarine Volcano	No	Ioto [Iwo-jima]	77	Caldera	No
8	Hunga Tonga-Hunga Ha'apai	20	Submarine Volcano	No	Falcon Island	40	Submarine Volcano	No	Unnamed (0403-03)	43	Submarine Volcano	No
*9	*Tavui*	37	Caldera	No	Rabaul	53	Pyroclastic Shield	Yes				
10	*Escanaba Segment*	85	Submarine Volcano	No								
11	*Tafahi*	28	Stratovolcano	No	Curacoa	46	Submarine Volcano	No	Tafu-Maka	66	Submarine Volcano	No
*12	Vailulu'u	0[b]	Submarine Volcano	Yes	*Ta'u*	42	Shield Volcano	No	*Ofu-Olosega*	61	Shield Volcanoes	No
*13	Vailulu'u	4	Submarine Volcano	Yes	*Ta'u*	45	Shield Volcano	No	*Ofu-Olosega*	64	Shield Volcanoes	No
*14	Vailulu'u	10	Submarine Volcano	Yes	*Ta'u*	55	Shield Volcano	No	*Ofu-Olosega*	70	Shield Volcanoes	No
*15	Vailulu'u	8	Submarine Volcano	Yes	*Ta'u*	49	Shield Volcano	No	*Ofu-Olosega*	67	Shield Volcanoes	No
*16	*Tavui*	32	Caldera	No	Rabaul	48	Pyroclastic Shield	Yes				
17												
*18	*Tavui*	35	Caldera	No	Rabaul	50	Pyroclastic Shield	Yes				
*19	Loihi	19	Submarine Volcano	Yes	Kilauea	73	Shield Volcano	Yes	Mauna Loa	91	Shield Volcano	No
*20	Smith Rock	10	Submarine Volcano	Yes	Bayonnaise Rocks	42	Submarine Volcano	No	*Myojin Knoll*	67	Submarine Volcano	No
21	Kuchinoerabu-jima	70	Stratovolcanoes	Yes	Kikai	73	Caldera	No	*Ibusuki Volcanic Field*	94	Calderas	No
22	*Zavodovski*	14	Stratovolcano	No	*Hodson*	38	Stratovolcano	No	*Leskov Island*	50	Stratovolcano	No
23	*Musa River*	36	Hydrothermal Field	No	*Madilogo*	62	Pyroclastic Cone	No	*Managlase Plateau*	69	Volcanic Field	No
24	Unnamed (0403-01)	16	Submarine Volcano	No	*Unnamed (0403-011)*	18	Submarine Volcano	No	Unnamed (0403-03)	44	Submarine Volcano	No
25	Tanaga	38	Stratovolcanoes	No	*Takawangha*	40	Stratovolcano	No	Gareloi	43	Stratovolcano	No
*26	Miyakejima	10	Stratovolcano	Yes	*Kozu-shima*	30	Lava Domes	No	*Nii-jima*	32	Lava Domes	No
*27	Miyakejima	4	Stratovolcano	Yes	*Mikura-jima*	27	Stratovolcano	No	*Kozu-shima*	39	Lava Domes	No
*28	Miyakejima	2	Stratovolcano	Yes	*Mikura-jima*	25	Stratovolcano	No	*Kozu-shima*	39	Lava Domes	No
*29	Miyakejima	6	Stratovolcano	Yes	*Mikura-jima*	26	Stratovolcano	No	*Kozu-shima*	42	Lava Domes	No
*30	Miyakejima	7	Stratovolcano	Yes	*Mikura-jima*	29	Stratovolcano	No	*Kozu-shima*	39	Lava Domes	No
*31	Miyakejima	6	Stratovolcano	Yes	*Mikura-jima*	28	Stratovolcano	No	*Kozu-shima*	40	Lava Domes	No
*32	Miyakejima	7	Stratovolcano	Yes	*Mikura-jima*	26	Stratovolcano	No	*Kozu-shima*	43	Lava Domes	No
*33	Miyakejima	8	Stratovolcano	Yes	*Mikura-jima*	30	Stratovolcano	No	*Kozu-shima*	39	Lava Domes	No
*34	Miyakejima	7	Stratovolcano	Yes	*Mikura-jima*	28	Stratovolcano	No	*Kozu-shima*	41	Lava Domes	No
*35	Miyakejima	5	Stratovolcano	Yes	*Mikura-jima*	28	Stratovolcano	No	*Kozu-shima*	38	Lava Domes	No
*36	Miyakejima	5	Stratovolcano	Yes	*Mikura-jima*	26	Stratovolcano	No	*Kozu-shima*	41	Lava Domes	No
*37	Miyakejima	7	Stratovolcano	Yes	*Mikura-jima*	26	Stratovolcano	No	*Kozu-shima*	43	Lava Domes	No
*38	Miyakejima	8	Stratovolcano	Yes	*Mikura-jima*	29	Stratovolcano	No	*Kozu-shima*	41	Lava Domes	No
*39	Miyakejima	3	Stratovolcano	Yes	*Mikura-jima*	27	Stratovolcano	No	*Kozu-shima*	35	Lava Domes	No
*40	Miyakejima	6	Stratovolcano	Yes	*Mikura-jima*	27	Stratovolcano	No	*Kozu-shima*	41	Lava Domes	No
*41	Miyakejima	10	Stratovolcano	Yes	*Kozu-shima*	31	Lava Domes	No	*Nii-jima*	33	Lava Domes	No
*42	Miyakejima	1	Stratovolcano	Yes	*Mikura-jima*	26	Stratovolcano	No	*Kozu-shima*	37	Lava Domes	No
*43	Miyakejima	7	Stratovolcano	Yes	*Mikura-jima*	31	Stratovolcano	No	*Kozu-shima*	35	Lava Domes	No
*44	Miyakejima	2	Stratovolcano	Yes	*Mikura-jima*	27	Stratovolcano	No	*Kozu-shima*	36	Lava Domes	No
*45	Miyakejima	6	Stratovolcano	Yes	*Mikura-jima*	29	Stratovolcano	No	*Kozu-shima*	37	Lava Domes	No
*46	Miyakejima	2	Stratovolcano	Yes	*Mikura-jima*	27	Stratovolcano	No	*Kozu-shima*	37	Lava Domes	No
*47	Miyakejima	4	Stratovolcano	Yes	*Mikura-jima*	27	Stratovolcano	No	*Kozu-shima*	38	Lava Domes	No
*48	Miyakejima	5	Stratovolcano	Yes	*Mikura-jima*	25	Stratovolcano	No	*Kozu-shima*	41	Lava Domes	No
*49	Miyakejima	7	Stratovolcano	Yes	*Mikura-jima*	31	Stratovolcano	No	*Kozu-shima*	37	Lava Domes	No
*50	Miyakejima	5	Stratovolcano	Yes	*Mikura-jima*	28	Stratovolcano	No	*Kozu-shima*	38	Lava Domes	No

Table 2. (continued)

Three Nearest Volcanoes Within 100 km of Shallow Vertical-CLVD Earthquakes												
No.	Volcano 1	D1 (km)	Type	Unrest?	Volcano 2	D2 (km)	Type	Unrest?	Volcano 3	D3 (km)	Type	Unrest?
*51	Miyakejima	4	Stratovolcano	Yes	*Mikura-jima*	27	Stratovolcano	No	*Kozu-shima*	38	Lava Domes	No
*52	Miyakejima	8	Stratovolcano	Yes	*Mikura-jima*	29	Stratovolcano	No	*Kozu-shima*	41	Lava Domes	No
*53	Miyakejima	5	Stratovolcano	Yes	*Mikura-jima*	26	Stratovolcano	No	*Kozu-shima*	41	Lava Domes	No
*54	Miyakejima	6	Stratovolcano	Yes	*Mikura-jima*	28	Stratovolcano	No	*Kozu-shima*	39	Lava Domes	No
*55	Miyakejima	11	Stratovolcano	Yes	*Mikura-jima*	33	Stratovolcano	No	*Nii-jima*	38	Lava Domes	No
*56	Miyakejima	11	Stratovolcano	Yes	*Nii-jima*	34	Lava Domes	No	*Kozu-shima*	35	Lava Domes	No
*57	Miyakejima	5	Stratovolcano	Yes	*Mikura-jima*	25	Stratovolcano	No	*Kozu-shima*	41	Lava Domes	No
*58	Miyakejima	7	Stratovolcano	Yes	*Mikura-jima*	31	Stratovolcano	No	*Kozu-shima*	34	Lava Domes	No
*59	Miyakejima	5	Stratovolcano	Yes	*Mikura-jima*	27	Stratovolcano	No	*Kozu-shima*	40	Lava Domes	No
*60	Miyakejima	6	Stratovolcano	Yes	*Mikura-jima*	30	Stratovolcano	No	*Kozu-shima*	35	Lava Domes	No
*61	Miyakejima	6	Stratovolcano	Yes	*Mikura-jima*	30	Stratovolcano	No	*Kozu-shima*	34	Lava Domes	No
*62	Miyakejima	7	Stratovolcano	Yes	*Mikura-jima*	26	Stratovolcano	No	*Kozu-shima*	43	Lava Domes	No
*63	Miyakejima	6	Stratovolcano	Yes	*Mikura-jima*	27	Stratovolcano	No	*Kozu-shima*	41	Lava Domes	No
*64	Miyakejima	8	Stratovolcano	Yes	*Mikura-jima*	28	Stratovolcano	No	*Kozu-shima*	42	Lava Domes	No
*65	Miyakejima	7	Stratovolcano	Yes	*Mikura-jima*	26	Stratovolcano	No	*Kozu-shima*	43	Lava Domes	No
*66	Miyakejima	5	Stratovolcano	Yes	*Mikura-jima*	26	Stratovolcano	No	*Kozu-shima*	41	Lava Domes	No
*67	Miyakejima	8	Stratovolcano	Yes	*Mikura-jima*	30	Stratovolcano	No	*Kozu-shima*	39	Lava Domes	No
*68	*Nii-jima*	16	Lava Domes	No	*Kozu-shima*	24	Lava Domes	No	Miyakejima	27	Stratovolcano	Yes
69	*Zavodovski*	9	Stratovolcano	No	*Hodson*	47	Stratovolcano	No	Protector Shoal	59	Submarine Volcano	No
*70	Nyamuragira	8	Shield Volcano	No	Nyiragongo	17	Stratovolcano	Yes	*Karisimbi*	37	Stratovolcano	No
71	Falcon Island	60	Submarine Volcano	No	Hunga Tonga-Hunga Ha'apai	71	Submarine Volcano	No	Unnamed (0403-03)	79	Submarine Volcano	No
*72	*Panarea*	11	Stratovolcano	Yes	Stromboli	16	Stratovolcano	Yes	*Lipari*	28	Stratovolcanoes	No
73	Unnamed (0403-01)	14	Submarine Volcano	No	*Unnamed (0403-011)*	18	Submarine Volcano	No	Unnamed (0403-03)	47	Submarine Volcano	No
74	*Masaraga*	73	Stratovolcano	No	Mayon	74	Stratovolcano	No	*Iriga*	81	Stratovolcano	No
75	Thule Islands	55	Stratovolcanoes	No	Bristol Island	86	Stratovolcano	No				
76	Thule Islands	29	Stratovolcanoes	No	Bristol Island	53	Stratovolcano	No				
*77	Cerro Azul	19	Shield Volcano	No	Sierra Negra	30	Shield Volcano	Yes	Alcedo	73	Shield Volcano	No
78	Smith Rock	21	Submarine Volcano	No	Bayonnaise Roks	39	Submarine Volcano	No	*Myojin Knoll*	63	Submarine Volcano	No
*79	Tungurahua	0[b]	Stratovolcano	Yes	*Licto*	39	Scoria Cones	No	*Chimborazo*	42	Stratovolcano	No
80												
81	Kita-Iwo-jima	16	Stratovolcano	No	Kaitoku Seamount	66	Submarine Volcano	No	Ioto [Iwo-jima]	87	Caldera	No
82	*North Vate*	89	Stratovolcanoes	No								
83	*Traitor's Head*	34	Stratovolcano	No	Yasur	86	Stratovolcano	Yes				
*84	*Curtis Island*	2	Submarine Volcano	Yes	*Macauley Island*	39	Caldera	No	Giggenbach	57	Submarine Volcano	No
*85	NW Rota-1	60	Submarine Volcano	Yes								
86	Unnamed (0403-01)	16	Submarine Volcano	No	*Unnamed (0403-011)*	17	Submarine Volcano	No	Unnamed (0403-03)	44	Submarine Volcano	No

[a]Three nearest volcanoes within 100 km of the 86 shallow vertical-CLVD earthquakes reported in Table 1. We report the names of the volcanoes in addition to the distances between the volcanoes and the earthquake centroid locations (D1-D3). Volcano names written in italic have last known eruptions before 1900. We also report the volcano type (morphology) and indicate whether the vertical-CLVD earthquakes occurred during documented episodes of volcanic unrest at each nearby volcano. An asterisk next to the event number in column 1 indicates that the earthquake occurred during an episode of unrest at a volcano within ~60 km. See text for details.

[b]Centroid location fixed to the volcano.

submarine caldera [*Bai and Greenhalgh*, 2005; *Itikarai*, 2008 as referenced in *Johnson et al*., 2010]. Rabaul, on the other hand, has erupted frequently in the last several hundred years. Seismic tomography indicates that Rabaul is underlain by two magma chambers, a shallow chamber extending from 2 to 4 km depth and a deeper chamber extending from 12 to 18 km depth [*Finlayson et al*., 2003; *Bai and Greenhalgh*, 2005; *Itikarai*, 2008; *Johnson et al*., 2010].

[45] The most recent episode of volcanic unrest at Rabaul began in 1971 and was characterized by uplift of the caldera interior and increased seismicity concentrated along an annular structure [*McKee et al*., 1984]. Beginning in September 1983, Rabaul experienced a seismic crisis during which tens of thousands of small magnitude, high-frequency earthquakes occurred along an outward-dipping ring-fault structure extending to 4–5 km [*McKee et al*., 1984; *Mori and McKee*, 1987; *Mori et al*., 1989; *Jones and Stewart*, 1997; *Itikarai*, 2008; *Johnson et al*., 2010]. The seismic crisis was accompanied by ~80 cm of uplift in the central part of the caldera, although it is debated whether the deformation was due to the pressurization of shallow magmatic or hydrothermal sources in the caldera block [*McKee et al*., 1984; *Mori and McKee*, 1987; *Geyer and Gottsman*, 2010], overpressure of a deep magma reservoir [*De Natale and Pingue*, 1993], or the partial intrusion of a dike along the ring-fault structure [*Saunders*, 2001, 2005]. After May 1985, seismicity decreased at Rabaul, and the volcano did not erupt until 1994.

[46] On 19 September 1994, Rabaul began an explosive phase that continues today. Initially, the explosive eruption occurred simultaneously at two volcanic cones, Tavurvur on the northeast side and Vulcan on the west side of the caldera. Activity at Vulcan ceased by 2 October 1994, although explosive eruptions at Tavurvur continue to occur intermittently. The first two vertical-CLVD earthquakes occur before the start of explosive activity in September 1994 and are not associated with increases in the rate of seismicity or other unusual activity at the volcano. The remaining two vertical-CLVD earthquakes occur after the start of the 1994 eruption and are associated with elevated seismicity and explosions at Tavurvur [*Smithsonian Institution*, 1995a, 1996b]. Leveling measurements indicate that the 1995 earthquake is associated with deflation, whereas the 1996 earthquake is associated with slight inflation of the central caldera block [*Smithsonian Institution*, 1995a, 1996b]. All four vertical-T earthquakes at Rabaul are temporally associated with volcanic unrest, with two earthquakes occurring before the start of the 1994 eruption and two occurring after. The earthquakes do not seem to be linked to a specific type of shallow eruptive activity in the caldera itself, which suggests a link to deformation at deeper levels of the volcano.

4.4. Vailulu'u

[47] Four M_W 4.8–4.9 vertical-P earthquakes with B or C-quality CMT solutions took place in the Samoa Islands on 10 and 11 January 1995 (Figure 9). These earthquakes have centroid locations within 10 km of Vailulu'u, a recently discovered massive submarine volcano with a 2 km wide caldera. Vailulu'u is believed to mark the current location of the Samoan hot spot [*Hart et al*., 2000]. The vertical-P earthquakes are spatially and temporally associated with an anomalous swarm of $m_b < 5.0$ earthquakes that occurred northwest

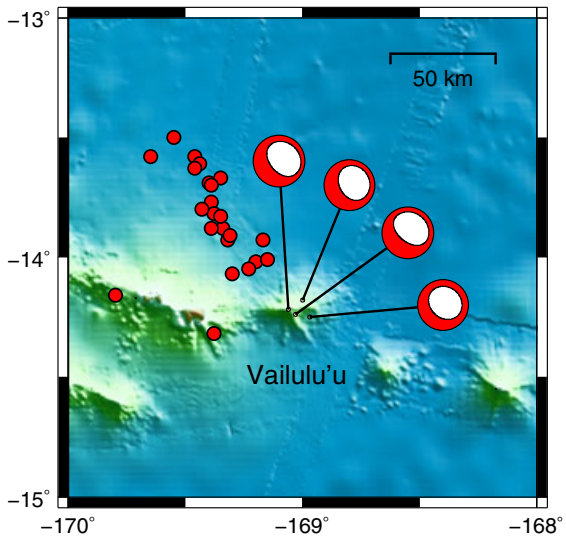

Figure 9. Map showing focal mechanisms for the four vertical-P earthquakes associated with an anomalous earthquake swarm that occurred at Vailulu'u volcano in January 1995. Red dots show the locations of $M > 4$ earthquakes from the NEIC catalog that occurred between 9 and 29 January 1995. Bathymetry is from the Global Multi-Resolution Topography (GMRT) synthesis [*Ryan et al*., 2009] used in GeoMapApp (http://www.geomapapp.org).

of the volcano from 9 to 29 January 1995. Acoustic *T* waves associated with the swarm were recorded by a local hydrophone array from 8 January to early February 1995 [*Smithsonian Institution*, 1995b]. Besides the January 1995 swarm, a search of the NEIC catalog (1973 to November 2012) finds no other examples of teleseismically detected earthquakes located within 100 km of Vailulu'u. Both the unusual locations of the January 1995 earthquakes and the fact that all of the earthquakes have similar magnitudes suggest that the swarm is associated with magmatic activity [*Konter et al*., 2004]. Indeed, radiometric ages of dredge samples from a 1999 cruise confirm that a volcanic eruption occurred in the summit crater of Vailulu'u within the prior 5–10 years [*Hart et al*., 2000]. The four events for which we have obtained CMT solutions show a clear association with this volcanic activity, occurring hours to days after the start of the volcanic earthquake swarm.

4.5. Loihi

[48] An M_W 4.9 vertical-T earthquake with a C-quality CMT solution occurred in Hawaii on 27 July 1996. The centroid location for this earthquake is ~20 km from Loihi, the youngest volcano in the Hawaiian chain. Loihi is a submarine volcano with a well-defined summit platform that contains several pit craters and an active hydrothermal system. On 16 July 1996, the largest earthquake swarm ever recorded in the Hawaiian Islands began at Loihi.

[49] The 1996 swarm can be divided into two distinct phases. The initial phase lasted from 16 to 18 July and was characterized by 170 $M_L > 1$ high-frequency volcano-tectonic earthquakes [*Caplan-Auerbach and Duennebier*, 2001]. After a brief hiatus on 19 January, when there were no locatable earthquakes at Loihi, the second phase commenced and the cumulative seismic moment increased dramatically. Thousands of earthquakes with magnitudes up to M_L 4.9 were located near Loihi through 9 August [*Duennebier et al*., 1997]. The second phase of the swarm, which consisted of predominantly long-period earthquakes, had two main pulses of activity, the first occurring between 20 and 25 July and the second occurring between 26 July and 5 August [*Caplan-Auerbach and Duennebier*, 2001]. The vertical-T earthquake occurred during the second pulse of seismic activity in Phase 2.

[50] Beginning on 6 August, submersible dives and bathymetry surveys confirmed that Pele's Peak, formerly the locus of Loihi's hydrothermal activity, had collapsed to form a new pit crater, Pele's Pit, with a diameter of 600 m and a depth of 300 m [*Duennebier et al*., 1997]. Although high-temperature hydrothermal plumes were observed, and popping noises were detected by sonobuoys, evidence of an ongoing eruption was not observed, and fresh lava recovered from the summit has been shown to predate the earthquake swarm by several months [*Duennebier et al*., 1997; *Garcia et al*., 1998, 2006]. The cause of the 1996 collapse of Pele's Pit is unknown, although it may have been triggered by a rapid draining of a shallow magma chamber, either into a volcanic rift zone or a deeper magma reservoir [*Davis and Clague*, 1998; *Caplan-Auerbach and Duennebier*, 2001]. The vertical-T earthquake, which occurred ~11 days after the start of the volcanic earthquake swarm, is clearly associated with this episode of volcanic activity and may have

been triggered either by rapid magma migration or the collapse of the pit crater.

4.6. Miyakejima

[51] Forty-three $4.4 \leq M_W \leq 5.6$ vertical-P earthquakes occurred in the Izu-Bonin volcanic arc between 7 July and 18 August 2000 (Figure 7). Most of the earthquakes have A-quality CMT solutions, although a few have B- or C-quality CMT solutions due to their small magnitudes or interference from other earthquakes. With the exception of the final earthquake, centroid locations for all of the vertical-P earthquakes are tightly clustered within ~10 km of Miyakejima, an 8 km wide volcanic island formed by a basaltic stratovolcano with several small summit calderas. In the summer of 2000, the most intense swarm of earthquakes ever observed in Japan began at Miyakejima and migrated northwestward to Kozushima, signaling the lateral propagation of a massive dike intrusion. Following a small submarine eruption, the summit crater of Miyakejima began to collapse on 8 July 2000. The collapse continued incrementally over a period of ~40 days, producing unusual tilt signals and the 43 vertical-P earthquakes. We summarize this eruptive activity below.

[52] On 26 June 2000, a swarm of small volcanic earthquakes was observed beneath Miyakejima's southwestern flank. Over a period of a few hours, seismicity intensified and migrated westward from the island, resulting in a small submarine eruption of basaltic andesite from four craters off the west coast of Miyakejima on 27 July [*Fujita et al*., 2001; *Sakai et al*., 2001; *Amma-Miyasaka et al*., 2005; *Kaneko et al*., 2005; *Uhira et al*., 2005]. Following the eruption, the swarm continued to migrate ~30 km northwestward and reached the area between Kozushima and Niijima islands by 1 July [*Sakai et al*., 2001; *Fujita et al*., 2001]. Intense seismicity was observed in the area between Miyakejima and Kozushima through September 2000, and over 600 $M \geq 4$ earthquakes and five $M \geq 6$ earthquakes were observed [*Ito and Yoshioka*, 2002; *Toda et al*., 2002; *Minson et al*., 2007]. Analysis of data from island GPS stations indicates that 1–2 km^3 of magma was intruded during this episode [*Nishimura et al*., 2001; *Toda et al*., 2002; *Ozawa et al*., 2004]. Crustal extension northwest of Miyakejima was coincident with contraction of the island, which indicates that a large portion of the magma was sourced from crustal magma chambers beneath the volcano, although additional magma may have been sourced from sub-crustal magma reservoirs located between Miyakejima and Kozushima [*Nishimura et al*., 2001; *Ozawa et al*., 2004; *Yamaoka et al*., 2005; *Murase et al*., 2006].

[53] Beginning on 4 July, seismicity beneath the summit area of Miyakejima was reactivated as the roof of the magma reservoir began to collapse [*Sakai et al*., 2001; *Nakada et al*., 2005]. As confirmed by gravity and electromagnetic data, shallowing seismicity resulted from the upward migration of a stoping column and the formation of a shallow cavity beneath the summit area [*Kikuchi et al*., 2001; *Geshi et al*., 2002; *Sasai et al*., 2002; *Furuya et al*., 2003]. On 8 July, coincident with a small phreatic eruption, an 800 m wide area of the summit collapsed ~200 m, producing a caldera with an initial volume of 5.6×10^7 m^3 [*Nakada et al*., 2005]. The caldera continued to collapse incrementally through mid-August, resulting in a 1.6 km wide depression with an average depth of 450 m [*Nakada et al*., 2005]. Small phreatic or phreatomagmatic eruptions took place along the southern rim of the volcano on 14–15 July, 10 August, and 13 August [*Nakada et al*., 2005; *Geshi and Oikawa*, 2008]. On 13 August, the composition of the erupted magma changed from basaltic andesite sourced from a shallow magma chamber at 3 to 5 km depth to basalt sourced from a deeper magma reservoir between 8 and 10 km depth [*Amma-Miyasaka et al*., 2005; *Kaneko et al*., 2005; *Saito et al*., 2005]. On 18 August, a vulcanian to subplinian eruption produced a 16 km high eruption column [*Nakada et al*., 2005]. After this eruption, large amounts of volcanic gases began to be emitted from the summit crater of Miyakejima, and the island was evacuated [*Kazahaya et al*., 2004].

[54] The caldera collapse of Miyakejima is believed to have been accommodated by slip on inward- and outward-dipping ring-fault structures [*Geshi et al*., 2002; *Geshi*, 2009]. Individual collapse episodes produced simultaneous tilt changes [*Ukawa et al*., 2000; *Yamamoto et al*., 2001] and variations in the electric and magnetic fields [*Sasai et al*., 2001; 2002], as well as, in most cases, very-long-period (VLP) seismic signals [*Kikuchi et al*., 2001; *Kumagai et al*., 2001]. In total, 46 major tilt steps were identified between the first explosive eruption on 8 July and the largest explosive eruption on 18 August [*Yamamoto et al*., 2001]. These tilt steps, which are characterized by an abrupt uplift of the summit area [*Ukawa et al*., 2000], have been variably explained by the opening of sill-like tensile cracks [*Fujita et al*., 2002, 2004] and the elastic response of the edifice to downward motion of the caldera block [*Michon et al*., 2009, 2011]. Thirty-nine of these tilt steps were also accompanied by regionally recorded VLP seismic pulses with durations of ~30–65 s [*Kikuchi et al*., 2001; *Kumagai et al*., 2001; *Ohminato and Kumagai*, 2001]. In several cases, the VLP pulses were preceded by swarms of shallow M1-2 earthquakes that increased in frequency before each event [*Kobayashi et al*., 2003]. Full-moment-tensor solutions for the VLP signals calculated by *Kikuchi et al*. [2001] and *Kumagai et al*. [2001] are dominated by positive volumetric components, and those events with larger volumetric changes tend to have longer recurrence intervals. So far, the VLP signals have been explained by piston collapse [*Kumagai et al*., 2001; *Stix and Kobayashi*, 2008] and a hydrothermal expansion model [*Kikuchi et al*., 2001]. However, a source process consisting of dip-slip motion on a caldera ring fault may be a viable alternative [*Ekström and Nettles*, 2002].

[55] All 43 vertical-P earthquakes we identify in this study occur after the start of the earthquake swarm and before the end of the incremental caldera collapse of Miyakejima. Thirty-nine of these vertical-P earthquakes correspond to the VLP signals described by *Kikuchi et al*. [2001] and linked by those authors to discrete collapse events. The four additional earthquakes we study occurred on 7, 9, and 30 July, and 18 August. The 7 July event is an M_W 4.4 earthquake that took place before the start of the caldera collapse. The remaining three earthquakes have magnitudes $4.8 \leq M_W \leq 5.5$ and are associated with observed tilt steps [*Fujita et al*., 2004]. The 18 August earthquake occurred during the climax of Miyakejima's largest explosive eruption [*Nakada et al*., 2005]. The centroid location for the 18 August earthquake is ~25 km away from Miyakejima, whereas all of the other events are within ~10 km of the volcano. CMT solutions with the centroid location fixed to the

volcano provide a poorer fit to the data, which may suggest that the final earthquake has a slightly different location or source process.

4.7. Nyiragongo

[56] As discussed in section 1, *Shuler and Ekström* [2009] identified five $4.6 \leq M_W \leq 5.3$ vertical-P earthquakes near Nyiragongo, a stratovolcano in the Democratic Republic of the Congo, between 2002 and 2005. The first three vertical-P earthquakes occurred on 21 and 22 January 2002, days after a regional rifting episode reopened fractures on the southern flanks of Nyiragongo and ruptured the volcanic edifice resulting in a catastrophic fissure eruption on 17 January [*Allard et al*., 2002; *Komorowski et al*., 2002/2003; *Tedesco et al*., 2007]. These three vertical-P earthquakes occurred between the end of the 12 h effusive eruption and the collapse of the summit crater, which had previously contained a solidified lava lake. These earthquakes are attributed to dip-slip motion along an inward-dipping ring fault located above a deflating shallow magma reservoir [*Shuler and Ekström*, 2009].

[57] The five earthquakes identified by *Shuler and Ekström* [2009] are Category 2 events from the Surface Wave catalog. Analysis of Category 1 earthquakes in this study allowed us to identify one additional vertical-P earthquake associated with the 2002 eruption, an M_W 5.1 earthquake that took place on 20 January 2002. This earthquake has a C-quality CMT solution and a centroid location ~15 km from Nyiragongo. This earthquake occurred before the three previously identified vertical-P earthquakes, between the end of the effusive eruption and the collapse of the summit crater, and can likely be explained by the same physical mechanism.

4.8. Stromboli

[58] An M_W 4.3 vertical-T earthquake with a C-quality CMT solution took place on 5 April 2003. The centroid location for this earthquake is ~15 km from Stromboli, the northernmost stratovolcano in the Aeolian Islands near Sicily, Italy. This earthquake occurred during the largest vulcanian eruption at Stromboli since 1930. This paroxysm was recorded by the local multiparametric monitoring network and directly observed from a helicopter.

[59] The 2003 paroxysm occurred during an effusive eruption at Stromboli that began in December 2002. An increased release of magmatic gases was observed in the month before the event, which likely indicates that gas-rich magma had ascended in the shallow plumbing system [*Aiuppa and Federico*, 2004; *Carapezza et al*., 2004; *Rizzo et al*., 2008]. Ash emission and temperature increase at the bottom of the obstructed summit craters were observed immediately before the paroxysm [*Calvari et al*., 2006]. Three minutes before the explosion, on 5 April 2003 at 7:10:25 UTC, the temperature of one summit crater increased dramatically and a thick gas plume was produced [*Calvari et al*., 2006]. At 7:13:05, reddish ash erupted and a dark cloud with a cauliflower shape grew above the crater [*Calvari et al*., 2006; *Rosi et al*., 2006; *Harris et al*., 2008]. After the initial explosion expanded to a second summit crater, a powerful blast produced a shock wave that was observed on a local seismic station at 7:13:37 [*Calvari et al*., 2006; *Harris et al*., 2008]. The 2003 paroxysm, which lasted 9 min, launched meter-sized ballistic blocks from the summit crater and produced an eruptive column that collapsed into pyroclastic flows [*Calvari et al*., 2006]. Like other paroxysms at Stromboli, the 2003 paroxysm erupted aphyric golden pumice, likely caused by the rapid ascent of undegassed basaltic magma [*Bertagnini et al*., 2003; *Métrich et al*., 2005; *Francalanci et al*., 2008; *Allard*, 2009].

[60] Broadband seismometers deployed on and around Stromboli clearly recorded the paroxysm. At 7:12:42, a high-frequency signal likely associated with vesiculation began, and at 7:13:35, a powerful 12 s VLP event was observed in association with the main blast [*D'Auria et al*., 2006; *Ripepe and Harris*, 2008]. A source inversion of the main blast signal retrieved a combination of a vertical-CLVD earthquake and a downward force with an equivalent magnitude of M_W 3.7 [*Cesca et al*., 2007]. Additionally, an ultra-long-period (ULP) signal starting 4 min before and terminating 1 min after the main blast was also observed [*Cesca et al*., 2007]. The ULP signal has been variably interpreted as tilt caused by the rapid ascent and ejection of magma [*D'Auria et al*., 2006] and as an M_W 3.0 slow thrust-faulting event [*Cesca et al*., 2007]. This signal is unlikely to be source of the vertical-T earthquake that we identify in this study because the amplitude of the ULP signal on the vertical component is more than an order of magnitude lower than the horizontal components. The vertical-T earthquake at Stromboli has a centroid time of 7:13:45.5, which suggests that the earthquake is associated with the VLP event and the main blast of the paroxysmal explosion.

4.9. Sierra Negra

[61] An M_W 5.5 vertical-T earthquake took place in the western Galápagos Islands on 22 October 2005. The centroid location for this event is immediately south of Isabela Island, ~30 km from Sierra Negra, the largest shield volcano in the Galápagos Islands. Sierra Negra has a subaerial extent of 60-by-40 km and contains a shallow 7-by-10 km summit caldera. The interior of Sierra Negra's caldera contains a 14 km long C-shaped sinuous ridge composed of tilted fault blocks with steeply dipping fault scarps [*Reynolds et al*., 1995]. It has been suggested that this fault system was formed by a series of repeated trapdoor-faulting events driven by magma accumulation [*Reynolds et al*., 1995; *Amelung et al*., 2000; *Jónsson et al*., 2005; *Chadwick et al*., 2006; *Jónsson*, 2009] in Sierra Negra's ~2 km deep sill-like magma chamber [*Amelung et al*., 2000; *Yun et al*., 2006]. During a trapdoor-faulting event, the crust above a shallow magma chamber is uplifted on one side of the caldera [*Amelung et al*., 2000].

[62] Trapdoor-faulting events in 1997–1998 and on 16 April 2005 are characterized by maximum uplift just north of the sinuous ridge in the southern part of the caldera [*Amelung et al*., 2000; *Jónsson et al*., 2005; *Chadwick et al*., 2006; *Jónsson*, 2009]. An m_b 4.6 earthquake is associated with the April 2005 trapdoor-faulting event, during which a GPS station located near the sinuous ridge was uplifted 84 cm within 10 s [*Chadwick et al*., 2006]. Although the 1997–1998 trapdoor-faulting event was originally attributed to slip along steep outward-dipping normal faults [*Amelung et al*., 2000], a revised faulting model consisting of 67°–74° inward-dipping thrust faults is compatible with the deformation data from both the 1997–1998

and April 2005 trapdoor-faulting events [*Chadwick et al*., 2006; *Jónsson*, 2009].

[63] On 22 October 2005 at 23:30 UTC, Sierra Negra began erupting after a repose period of 26 years. The start of the eruption was accompanied by a 13 km high plume of ash and steam, after which the eruption transitioned to a 2 km long curtain of fire fountains inside the northern rim of the caldera [*Geist et al*., 2008]. Over the next 8 days, $\sim 150 \times 10^6\,m^3$ of basalt was erupted and the center of the caldera subsided over 5 m [*Yun*, 2007; *Geist et al*., 2008]. No precursors to the eruption were observed, except for the M_W 5.5 vertical-T earthquake that occurred at 20:34 on 22 October. Unfortunately, the GPS network failed 16 h prior to the start of the eruption so deformation associated with this event is poorly constrained [*Geist et al*., 2008]. *Yun* [2007] modeled interferograms that span the earthquake and the eruption and found that the deformation can be explained by a model that includes a trapdoor-faulting event centered on the western part of the sinuous ridge. The 1.5 m of maximum dip-slip at the surface estimated by *Yun* [2007] is consistent with field measurements of dip-slip displacements on vertical fault scarps in the southern and western parts of the sinuous ridge [*Geist et al*., 2008]. The vertical-T earthquake, which occurred ~3 h before the start of the 2005 eruption, may be associated with a trapdoor-faulting event.

4.10. Tungurahua

[64] An M_W 4.4 vertical-P earthquake with a C-quality CMT solution took place in Ecuador on 17 August 2006. The centroid location for this earthquake is ~25 km from Tungurahua, one of the most active volcanoes in the Andes [*Hall et al*., 1999]. Tungurahua is a large andesitic stratovolcano that has been erupting intermittently since 1999. In 2006, explosive eruptions on 14 July and 16–17 August produced widespread pyroclastic flows, resulting in loss of life and the evacuation of settlements along the flanks of the volcano. The vertical-P earthquake occurred during the paroxysmal phase of the VEI 3 (Volcanic Explosivity Index) [*Newhall and Self*, 1982] 16–17 August eruption, Tungurahua's most violent eruption since activity began in 1999.

[65] The August 2006 eruption was preceded by the growth of a bulge on the northern flank of the volcano between 11 and 16 August [*Smithsonian Institution*, 2006] and by 16 h of uninterrupted, escalating seismic tremor and tephra fallout [*Arellano et al*., 2008]. The eruption began on 16 August at 19:30 UTC, and by 22:00, lava fountains reached a height of 100–200 m above the vent [*Barba et al*., 2006]. Around 3:00 on 17 August, numerous pyroclastic density currents were observed [*Barba et al*., 2006] and the ash plume rose to a height of 13.25 km [*Fee et al*., 2010]. Between 4:00 and 5:00, the lava fountains reached ~1.5 km, and at ~5:30 the start of the paroxysmal phase of the eruption began [*Barba et al*., 2006; *Fee et al*., 2010]. The vertical-P earthquake took place shortly thereafter, at 5:37 UTC.

[66] The paroxysmal phase of the 16–17 August eruption lasted 50 min and was characterized by a dramatic increase in acoustic power, as well as a shift in the infrasonic jetting spectrum toward lower frequencies [*Matoza et al*., 2009; *Fee et al*., 2010]. The height of the ash cloud grew to over 24 km, and ash was injected into the stratosphere while lava fountaining continued at heights of over 1 km [*Fee et al*., 2010; *Steffke et al*., 2010]. Numerous pyroclastic density currents and heavy ashfall were observed [*Barba et al*., 2006]. At 6:20, the eruptive activity dropped off sharply and by ~7:30, the tremor was at background levels [*Fee et al*., 2010]. In total, the eruption lasted 11 h, and produced $2 \times 10^7\,m^3$ of magma and 35,000 t of SO_2 [*Arellano et al*., 2008; *Carn et al*., 2008; *Fee et al*., 2010]. Hours after the end of the eruption, the effusion of slow-moving blocky lava flows was observed [*Arellano et al*., 2008; *Hanson et al*., 2011; *Samaniego et al*., 2011]. It has been suggested that the end of the August 2006 eruption may have resulted from the slow ascent of a more viscous magma [*Hanson et al*., 2011].

[67] A series of VLP events was observed during the August 2006 eruption [*Kumagai et al*., 2007a, 2007b, 2010]. These events started at 5:30 UTC on 17 August and are characterized by impulsive signatures with dominant periods of 20–50 s [*Kumagai et al*., 2007b]. The vertical-P earthquake that we identify in this study is likely the same event as "VLP2" from *Kumagai et al*. [2010]. In a waveform inversion using seismic data from two local broadband stations, *Kumagai et al*. [2010] modeled this event as an isotropic source at 3 km depth and hypothesized that the volumetric change was caused by bubble growth due to newly supplied magma. However, it seems possible that the vertical-P earthquake, which occurred during the paroxysmal phase of the explosive eruption, could have been generated by a collapse inside the magmatic plumbing system, as at Nyiragongo and Miyakejima.

4.11. Curtis Island

[68] On 17 February 2009, the largest well-documented vertical-CLVD earthquake, an M_W 5.8 vertical-T event took place in the Kermadec Islands north of New Zealand. The centroid location is ~2 km from Curtis Island. Together with Cheeseman Island, Curtis Island is the subaerial portion of a submarine dacitic volcano located along the Kermadec Ridge [*Doyle et al*., 1979; *Smith et al*., 1988]. Curtis Island has a subaerial extent of 500-by-800 m and contains a crater with active fumaroles. Although uplift of 7 m was documented at Curtis Island between 1929 and 1964 [*Doyle et al*., 1979], the date of Curtis Island's last eruption is unknown. From 17 to 19 January 2009, earthquakes with *T*-wave phases were recorded on the Polynesian seismic network [*Smithsonian Institution*, 2009], suggesting a possible eruption near the volcano. As Curtis Island is a remote volcano, this activity was not confirmed. Because no thermal alerts were issued by the MODVOLC system [*Wright et al*., 2002, 2004] through April 2009 [*Smithsonian Institution*, 2009], the vertical-T earthquake, which occurred 1 month after the T waves were observed, is likely associated with magma migration within the volcanic edifice or magmatic plumbing system of Curtis Island rather than a volcanic eruption.

4.12. NW Rota-1

[69] On 19 April 2009, an M_W 4.9 vertical-P earthquake with a C-quality CMT solution took place in the Mariana Islands. The centroid location for this earthquake is ~60 km from NW Rota-1, a recently detected submarine volcano with an active hydrothermal system [*Embley et al*., 2006].

NW Rota-1 is a steep-sided basaltic to basaltic-andesitic cone with a diameter of 16 km and a summit depth of ~500 m [*Embley et al*., 2006; *Chadwick et al*., 2008]. In 2004, the first explosive submarine eruptions ever to be observed were witnessed at NW Rota-1 [*Embley et al*., 2006]. Repeated dives indicate eruptive activity is characterized by nearly continuous Strombolian eruptions [*Chadwick et al*., 2008].

[70] In mid-April 2009, an unusual sequence of $m_b \leq 5.0$ earthquakes near NW Rota-1 was detected by both the NEIC and a hydrophone moored in the summit of the volcano [*Chadwick et al*., 2012]. The peak seismicity was observed on 17 April, the first day of the 4 day swarm, when the hydrophone recorded a continuous broadband acoustic signal that lasted for ~24 h [*Chadwick et al*., 2012]. The vertical-P earthquake occurred ~2 days after the beginning of the swarm. The April 2009 swarm closely resembles another earthquake sequence that occurred near NW Rota-1 in 1997, and both swarms have been attributed to magmatic sources [*Heeszel et al*., 2008; *Chadwick et al*., 2012]. Four months after the swarm, in August 2009, a large volcanic eruption and subsequent landslide took place at NW Rota-1 [*Chadwick et al*., 2012]. The relative timing of the earthquake swarm and the eruption suggests that the vertical-P earthquake may be associated with a magmatic intrusion or the inflation of a shallow magma chamber.

4.13. Other Vertical-CLVD Earthquakes

[71] The remaining 24 vertical-CLVD earthquakes identified in this study are not associated with documented episodes of volcanic unrest at nearby volcanoes. Several of these earthquakes occur in spatial clusters near individual volcanoes. We summarize the locations of the vertical-CLVD earthquakes, starting in Cascadia and moving counterclockwise around the Pacific Ocean. Unless otherwise indicated, the earthquakes have A-quality CMT solutions.

[72] An M_W 4.7 vertical-P earthquake with a B-quality CMT solution took place on 19 March 1994 along the Gorda Ridge, north of the Mendocino Fracture Zone off the coast of Oregon. This earthquake occurred near the boundary between the Central and Phoenix ridge segments and is not associated with any unusual earthquake swarms or reported eruptions along either segment.

[73] On 4 December 1999, an M_W 5.1 vertical-P earthquake with a B-quality CMT solution occurred in the Andreanof Islands in the central Aleutians. The centroid location for this earthquake is ~40 km from Tanaga, Takawangha, and Gareloi volcanoes. All three of these volcanoes are stratovolcanoes. Tanaga last erupted in 1914, and Gareloi last erupted in 1989. Takawangha has no known historical eruptions, although radiocarbon data indicates that explosive eruptions have occurred there in the past several hundred years [*Siebert and Simkin*, 2002-].

[74] Four vertical-CLVD earthquakes that are not associated with volcanic unrest took place in Japan. The first earthquake is an M_W 5.3 vertical-T earthquake that occurred on 16 May 1978 in Northern Honshu near Hokkaido. This earthquake is not located near any recently active volcanoes, but the centroid location is ~40 km from Osore-yama, a historically active stratovolcano with a 5 km wide caldera.

[75] An M_W 5.7 vertical-P earthquake occurred on 9 September 1996 in the Ryukyu Islands near Kyushu. The centroid location for this earthquake is ~70 km from Kuchinoerabu-jima and Kikai volcanoes. Kikai is a 19 km wide caldera that erupted in 1997 and 1998. Kuchinoerabu-jima is a group of young stratovolcanoes that produces frequent explosive eruptions. The vertical-P earthquake occurred during a seismic swarm at Kuchinoerabu-jima [*Iguchi et al*., 2001]. However, an earthquake aftershock survey by *Sekitani et al*. [1997] confirms that the earthquake we study occurred on Tanegashima Island, ~60 km east of the volcanic arc. Therefore, it seems unlikely that this earthquake is associated with the Kuchinoerabu-jima magmatic activity.

[76] Two M_W 5.2-5.3 vertical-T earthquakes have centroid locations ~15 km from Kita-Iwo-jima, a deeply eroded stratovolcano in Japan's Volcano Islands. The first earthquake occurred on 20 August 1992 and the second earthquake occurred on 12 June 2008. Numerous eruptions have been reported from Funka-Asane, a submarine vent located 2 km northwest of Kita-Iwo-jima, but no eruptions were reported during the times of the vertical-T earthquakes.

[77] An M_W 4.7 vertical-P earthquake with a C-quality CMT solution took place on 11 April 2008 in the Mariana Islands. The centroid location for this earthquake is ~110 km west of the volcanic arc and is likely associated with the Mariana Trough, an actively spreading back-arc basin separating the Mariana Ridge, a remnant volcanic arc, from the active volcanoes of the Mariana Arc. No volcanic activity has been reported at this location near the time of the earthquake.

[78] On 25 February 2005, an M_W 4.9 vertical-P earthquake with a B-quality CMT solution occurred in Luzon in the Philippines. The centroid location for this earthquake is ~75 km from Masaraga and Mayon volcanoes. Masaraga is a Holocene stratovolcano, and Mayon is a stratovolcano that has frequent explosive eruptions. Mayon had small-scale explosive eruptions from June to September 2004, but was not erupting during the time of the vertical-P earthquake.

[79] An M_W 5.6 vertical-P earthquake with a B-quality CMT solution took place on 29 June 1999 in east Papua New Guinea. The centroid location for this earthquake is ~35 km from an active hydrothermal field called Musa River, ~60 km from Madilogo, a Holocene pyroclastic cone, and ~70 km from Managlase Plateau, a Holocene volcanic field. The earthquake is also located ~75 km from Lamington, a stratovolcano that last erupted in 1956. The vertical-P earthquake is not linked to unrest at any of these volcanoes.

[80] Two vertical-CLVD earthquakes with C-quality CMT solutions occurred in the Vanuatu Islands region in 2008. The first earthquake is an M_W 4.9 vertical-T earthquake that took place on 22 July 2008. The centroid location for this earthquake is ~90 km from North Vate, a Holocene stratovolcano. The second earthquake is an M_W 5.0 vertical-T earthquake that occurred on 18 November 2008. The centroid location for this earthquake is ~35 km from Traitor's Head, a historically active stratovolcano, and ~85 km from Yasur, a stratovolcano that was producing continuous strombolian and vulcanian eruptions during this time. We do not link the 18 November 2008 earthquake to the volcanic activity at Yasur due to the large distance between the centroid location and the volcano.

[81] Eight vertical-CLVD earthquakes, three vertical-P and five vertical-T events, are located in the Tonga and Fiji

Islands region. The vertical-P earthquakes occurred between 1994 and 2002. The first event is an M_W 4.8 earthquake with a B-quality CMT solution that occurred near the Mangatolo Triple Junction on 8 November 1994. The centroid location for this earthquake is ~30 km from Tafahi, a Holocene stratovolcano, and ~45 km from Curacoa, a submarine volcano that last erupted in 1979. The second event is an M_W 4.8 earthquake with a C-quality CMT solution that occurred on 9 September 1995 along the Fonualei Rift and Spreading Center (FRSC). The third event is an M_W 4.7 earthquake with a C-quality CMT solution that occurred on 16 August 2002. The centroid location for this earthquake is ~60 km from Falcon Island, a submarine volcano that last erupted in 1936, and ~70 km from Hunga Tonga-Hunga Ha'apai, a submarine volcano that erupted in 1988 and 2009. None of the vertical-P earthquakes are linked to documented episodes of volcanic unrest.

[82] The five vertical-T earthquakes that took place in the Tonga and Fiji Islands regions occurred over a 20 year period between 1979 and 2009. The northernmost earthquake is an M_W 5.3 earthquake that took place on 16 January 1994. The centroid location for this earthquake is ~20 km from Hunga Tonga-Hunga Ha'apai, a submarine volcano with a 4–5 km wide caldera that experienced a Surtseyan eruption in March 2009 [*Vaughan and Webley*, 2010]. The remaining four events are M_W 5.5 earthquakes that occurred on 1 October 1979, 7 August 1999, 10 November 2004, and 26 May 2009. The 1979 earthquake has a B-quality CMT solution and the three other earthquakes have A-quality CMT solutions. All four of these vertical-T earthquakes have centroid locations clustered ~10–15 km from an Unnamed submarine volcano (0403-01 in IAVCEI's Catalog of Active Volcanoes of the World). The last confirmed eruption from Unnamed volcano (0403-01) was in 1932. The centroid locations for these earthquakes are also ~20 km from Unnamed volcano (0403-011), a Holocene submarine volcano, and ~45–50 km from Unnamed volcano (0403-03), a submarine volcano that last erupted in 1999. None of these vertical-T events are associated with documented eruptive activity.

[83] Finally, five vertical-T earthquakes are located in the remote South Sandwich Islands. Three M_W 5.3–5.4 earthquakes took place in the northern South Sandwich Islands on 9 September 1978, 5 September 1997, and 18 January 2001. These earthquakes have A- or B-quality CMT solutions and centroid locations that are clustered within ~15 km of Zavodovski, the northernmost subaerial volcano in the South Sandwich Islands. Zavodovski is a stratovolcano with active fumaroles that last erupted in 1819. Centroid locations for these earthquakes are also ~40 km from Hodson, a Holocene stratovolcano. The remaining two vertical-T earthquakes took place in the southern South Sandwich Islands on 23 and 31 August 2005. Centroid locations for these M_W 5.1 and M_W 5.5 earthquakes are located ~30 and ~55 km from Thule Islands volcanoes. The Thule Islands consist of a group of stratovolcanoes and calderas that have produced several explosive eruptions in the last hundred years. The 2005 earthquakes also have centroid locations ~50 km and ~85 km from Bristol Island, a historically active stratovolcano that last erupted in 1956. None of the vertical-T earthquakes in the South Sandwich Islands are associated with documented volcanic unrest, although visual observations of the South Sandwich Islands are limited to a few days each year [*LeMasurier et al*., 1990].

5. Discussion

[84] After investigating 395 target earthquakes located within 100 km of volcanoes with documented eruptions in the last ~100 years, we have identified 86 shallow vertical-CLVD earthquakes with magnitudes $4.3 \leq M_W \leq 5.8$. Of the vertical-CLVD earthquakes investigated in this study, we find that ~80% are located within 30 km and ~90% are located within 50 km of a known volcanic center. For those earthquakes that are linked to documented episodes of volcanic unrest at active volcanoes, ~90% are located within 30 km of the source volcano, and the farthest earthquake is located ~60 km away. Even for vertical-CLVD earthquakes that are not linked to episodes of volcanic unrest, ~50% are located within 30 km of a known volcano. The vertical-CLVD earthquakes are associated with more than 20 active volcanoes around the world.

[85] The vertical-CLVD earthquakes identified in this study all have shallow depths. During the CMT inversion process, all of the centroid depths were fixed by the inversion algorithm to 12 km to prevent them from moving shallower, and body-wave modeling of 18 earthquakes, all from the GCMT catalog, suggests that the vertical-CLVD earthquakes occur in the top 10 km of the crust. Given that most vertical-CLVD earthquakes are tightly clustered around active volcanoes, the shallow depth estimates suggest that they are likely associated with deformation inside or immediately beneath volcanic edifices.

[86] Overall, ~70% of the vertical-CLVD earthquakes identified in this study are spatially and temporally associated with documented volcanic unrest. Breaking this down by earthquake type, ~40% of vertical-T earthquakes and ~85% of vertical-P earthquakes are linked to volcanic unrest. If the earthquakes associated with the Miyakejima caldera collapse are excluded, ~45% of the remaining vertical-P earthquakes occur during documented episodes of volcanic unrest at a nearby volcano. Volcanic unrest is underreported, especially in remote regions and in cases where unrest is not soon followed by an eruption [*Moran et al*., 2011], so the percentage of vertical-CLVD earthquakes associated with volcanic activity is likely to be even higher than is documented here. Most shallow vertical-CLVD earthquakes located near volcanoes are thus likely related to some type of volcanic unrest.

[87] Shallow vertical-CLVD earthquakes near recently active volcanoes represent a small fraction of earthquakes described in the GCMT and Surface Wave catalogs. Including events analyzed by *Nettles and Ekström* [1998], only ~0.1% of earthquakes described in the GCMT catalog from 1976 to 2009 are shallow vertical-CLVD earthquakes located near recently active volcanoes. Likewise, including events analyzed by *Shuler and Ekström* [2009], only ~2% of Category 1 and 2 earthquakes in the Surface Wave catalog from 1991 to 2009 are shallow vertical-CLVD earthquakes located near recently active volcanoes. Considering that at least 20 volcanoes around the world are erupting at any given time, it is clear that not all types of volcanic activity produce vertical-CLVD earthquakes. Certain stress and/or structural conditions may be required to generate this type of earthquake.

Below we examine potential correlations between vertical-CLVD earthquakes and tectonic setting as well as volcano type.

[88] Shallow vertical-CLVD earthquakes are located near volcanoes in many tectonic and geographic settings. The majority of vertical-CLVD earthquakes are located near arc volcanoes in subduction zones, mostly in the circum-Pacific region. Although many vertical-CLVD earthquakes are located in subduction zones along the western rim of the Pacific Ocean, and few vertical-CLVD earthquakes are located in South or Central America, or in the Cascade, Aleutian, or Kurile-Kamchatka arcs, there does not seem to be an obvious link between the age, geometry, or velocity of subducting slabs reported by *Syracuse and Abers* [2006] and the occurrence of vertical-CLVD earthquakes. Vertical-CLVD earthquakes are also associated with hot spot volcanoes in Iceland, Hawaii, the Samoa Islands, and the Galápagos Islands, as well as with volcanoes in the East African Rift.

[89] Only a very small number of vertical-CLVD earthquakes, all of the vertical-P type, are located along mid-ocean ridge segments. Included in this category are the 19 March 1994, 9 September 1995, and 11 April 2008 earthquakes. The centroid locations of these earthquakes are over 80 km away from the nearest recently active volcano. The locations of these earthquakes, which are along back-arc or mid-ocean ridge segments, suggest that these events may be associated with extension processes rather than directly with volcanic processes. The small number of vertical-CLVD earthquakes located along mid-ocean ridges is partly the result of the fact that we identified target earthquakes using the database of the GVP, which contains few submarine volcanoes located along divergent plate boundaries. However, there is some evidence that vertical-CLVD earthquakes may be less likely to occur in the ridge environment. A search through the entire GCMT catalog for shallow vertical-CLVD earthquakes with $|\varepsilon| > 0.33$ and dominant *P* or *T* axes that plunge more steeply than 60° finds only 15 earthquakes located along the mid-ocean ridge system. All of the earthquakes are vertical-P events. Given our experience with how the addition of surface-wave data affects CMT solutions (section 3.1 and Figure 4), it is possible that many of these events are poorly resolved normal-faulting earthquakes.

[90] Vertical-CLVD earthquakes are most commonly associated with submarine volcanoes and stratovolcanoes (Table 2). Additionally, most of the submarine volcanoes and stratovolcanoes closest to vertical-CLVD earthquakes have pre-existing calderas [*Siebert and Simkin*, 2002-]. In fact, the largest sequence of vertical-CLVD earthquakes is associated with the development of a new caldera at Miyakejima. Vertical-CLVD earthquakes are also associated with unrest at Rabaul, a pyroclastic shield volcano, and Sierra Negra, a shield volcano. Both of these shield volcanoes have calderas with well-documented ring-fault structures. Since ring faults are produced during the caldera collapse process, the fact that we observe most vertical-CLVD earthquakes at volcanoes with calderas may indicate that vertical-CLVD earthquakes are generated by slip on ring-fault structures.

[91] Most volcanoes associated with vertical-CLVD earthquakes erupt basaltic and/or andesitic lavas [*Siebert and Simkin*, 2002-]. Nyiragongo and Ol Doinyo Lengai, the two volcanoes associated with vertical-CLVD earthquakes in the East African rift, erupt lavas with some of the lowest known silica contents on Earth [*Sahama*, 1973; *Bailey*, 1993; *Demant et al*., 1994]. The correlation between vertical-CLVD earthquakes and basaltic-to-andesitic volcanoes may suggest that vertical-CLVD earthquakes preferentially occur at volcanoes that erupt low-viscosity magmas. However, this observation may also be a consequence of the relatively short time period covered by our study since basaltic volcanoes tend to erupt small volumes of lava frequently, whereas silicic volcanoes have longer repose periods and larger, less frequent eruptions [*White et al*., 2006].

[92] Vertical-CLVD earthquakes are observed during many different types of volcanic unrest. Half of all the vertical-CLVD earthquakes identified in this study are associated with the caldera collapse of Miyakejima. Vertical-CLVD earthquakes are also associated with a subglacial fissure eruption at Bárdarbunga, a fissure eruption at Nyiragongo, elevated seismicity and explosive eruptions at Rabaul, an effusive eruption at Sierra Negra, and explosive eruptions at Stromboli and Tungurahua. At submarine volcanoes, vertical-CLVD earthquakes are associated with anomalous earthquake swarms at Vailulu'u, Loihi, NW Rota-1, and Curtis Island, as well as disproportionately large tsunamis at Smith Rock.

[93] In Figure 10, we examine the temporal relationships between vertical-CLVD earthquakes and volcanic unrest at 10 volcanoes. We plot vertical-CLVD earthquakes that occurred within 5 years of the start of volcanic eruptions or episodes of unrest at each volcano. For some volcanoes, defining the start of an episode of unrest is arbitrary, but we use the following dates and times: (1) Bárdarbunga—30 September 1996, 23:30 UTC [*Smithsonian Institution*, 1996a]; (2) Loihi—17 July 1996, 7:54 UTC; (3) Miyakejima—26 June 2000, 9:00 UTC [*Nishimura et al*., 2001]; (4) NW Rota-1—17 April 2009, 4:43 UTC; (5) Nyiragongo—17 January 2002, 6:25 UTC [*Tedesco et al*., 2007]; (6) Rabaul—18 September 1994, 20:00 UTC [*Smithsonian Institution*, 1994]; (7) Sierra Negra—22 October 2005, 23:30 UTC [*Geist et al*., 2008]; (8) Stromboli—5 April 2003, 7:13 UTC [*Calvari et al*., 2006]; (9) Tungurahua—16 August 2006, 19:30 UTC [*Fee et al*., 2010]; and (10) Vailulu'u—9 January 1995, 14:13 UTC. For Loihi, NW Rota-1, and Vailulu'u, we use the NEIC catalog and define the start of volcanic unrest as the time of the first teleseismically-detected earthquake in each swarm.

[94] Vertical-P earthquakes occur hours to years after the start of eruptions or episodes of unrest, whereas vertical-T earthquakes occur both before and after eruptive activity. At Sierra Negra, a vertical-T earthquake preceded the 2005 eruption by 3 h, while at Bárdarbunga, a series of vertical-T earthquakes took place over 20 years, with the last occurring ~1.5 days before the 1996 subglacial eruption. These results suggest that vertical-CLVD earthquakes may be used to infer the eruptive states of volcanoes. In particular, vertical-P earthquakes may be used to identify volcanoes where eruptions or large-scale magmatic intrusions have recently occurred. This may be especially useful for remote or submarine volcanoes. In addition, vertical-T earthquakes may be used to identify volcanoes that are likely to erupt in the near future. Clusters of vertical-T earthquakes are located at Kita-Iwo-jima, Unnamed (0403-01), and Zavodovski

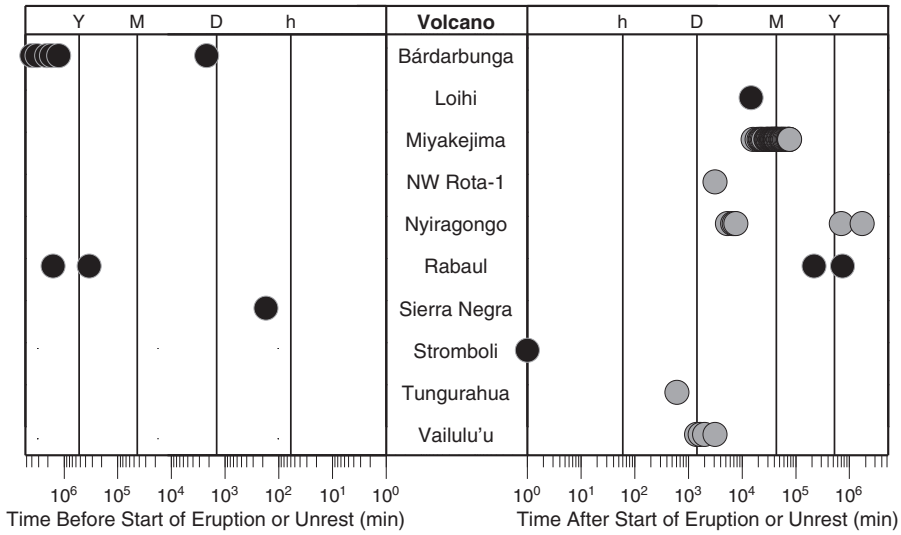

Figure 10. Plot showing the temporal relationships between vertical-CLVD earthquakes and volcanic unrest at 10 volcanoes. We plot 5 years of time (in min) before and after the start of eruptions or episodes of unrest. Vertical lines indicate 1 hour (*h*), 1 day (*D*), 1 month (*M*), and 1 year (*Y*). Vertical-P earthquakes are plotted as grey circles and vertical-T earthquakes are plotted as black circles. Earthquakes from Bárdarbunga are from *Nettles and Ekström* [1998], and earthquakes from Nyiragongo are from *Shuler and Ekström* [2009]. See the text for details on the dates and times of eruptions and episodes of volcanic unrest. Note that the vertical-T earthquake at Stromboli is plotted at 1 min after the start of the eruption, although it actually occurred only a few seconds later.

volcanoes, and these earthquakes may be indicative of magma ascent and increased potential for eruptions at these volcanoes.

6. Conclusions

[95] Through an in-depth analysis of two global seismicity catalogs and the calculation of over 300 CMT solutions, we have identified 86 shallow vertical-CLVD earthquakes occurring near recently active volcanoes. These earthquakes have depths in the upper 10 km of the crust, and 80% are located within 30 km of a volcano. Additionally, ~70% of the vertical-CLVD earthquakes studied are spatially and temporally associated with volcanic unrest at a nearby volcano. Half of the vertical-CLVD earthquakes are associated with the caldera collapse of Miyakejima in 2000, and another 20% are linked to documented volcanic unrest or eruptions at other volcanoes. In addition to caldera collapse, vertical-CLVD earthquakes are associated with effusive and explosive eruptions and volcanic earthquake swarms. There is thus a clear link between the occurrence of vertical-CLVD earthquakes and volcanic activity. Our observations suggest that these unusual earthquakes likely occur within the edifices or magmatic plumbing systems of active volcanoes.

[96] Vertical-CLVD earthquakes do not occur at all volcanoes, or even during all episodes of unrest at volcanoes where they are observed, so specific stress or structural conditions must be required to trigger these earthquakes. We have identified several correlations between the occurrence of vertical-CLVD earthquakes and specific tectonic settings and volcano types. Vertical-CLVD earthquakes are predominantly located in subduction zones, although they also occur in continental rifts and in areas of hot spot volcanism. Most vertical-CLVD earthquakes are associated with volcanoes with caldera structures. Additionally, most vertical-CLVD earthquakes are associated with volcanoes that erupt silica-poor magmas. These correlations may indicate that low-viscosity magmas and/or ring-fault structures are required to generate vertical-CLVD earthquakes.

[97] We examined the temporal relationships between vertical-CLVD earthquakes and volcanic unrest at 10 volcanoes and found that vertical-P earthquakes occur after the start of volcanic unrest, whereas vertical-T earthquakes generally occur before volcanic eruptions. The occurrence of vertical-P earthquakes may be useful for identifying remote or submarine volcanoes that have recently erupted, and the occurrence of vertical-T earthquakes may signal that a source volcano is likely to erupt in the future. Vertical-CLVD earthquakes provide information about the stress and strain conditions internal to active volcanoes, and by studying these rare and unusual earthquakes, we may learn more about the deformation processes occurring inside active volcanoes during eruptions and magma ascent and migration. Because vertical-CLVD earthquakes are associated with many different types of volcanic unrest, it is likely that these events can be produced by multiple physical processes. Constraining the physical mechanisms that may be responsible for generating vertical-CLVD earthquakes will enable us to interpret these events in terms of related volcanic hazards.

[98] **Acknowledgments.** We thank S. J. Saunders and W. W. Chadwick, Jr. for helpful comments and discussions. We thank Douglas Dreger and Hrvoje Tkalčić for providing thorough and constructive reviews that improved the clarity and quality of our manuscript. We are grateful to the operators of the Modified High Gain Long Period Observatory, the Black Forest Observatory, the China Digital Seismic Network, the Canadian National Seismic Network, the Czech Seismic Network, the

Digital World-Wide Standardized Seismographic Network, GEOSCOPE, GEOFON, High-Gain Long-Period Network, MEDNET, the Singapore Seismological Network, the Regional Seismic Test Network, the Seismic Research Observatory, TERRAscope, and the IRIS-USGS Global Seismographic Network for the collection of the seismic data used in this study. We also thank the IRIS Data Management Center for archiving and distributing these data. This project was supported by National Science Foundation award EAR-0944055 and EAR-0824694. AS was also supported by an NSF Graduate Research Fellowship.

References

Abe, K. (1988), Tsunami magnitude and the quantification of earthquake tsunamis around Japan, *Bull. Earthquake Res. Inst. Univ. Tokyo*, *63*, 289-303.

Acocella, V. (2008), Structural development of calderas: A synthesis from analog experiments, in *Caldera Volcanism: Analysis, Modelling and Response*, *Developments in Volcanology*, vol. 10, edited by J. Gottsman and J. Marti, pp. 285–311, Elsevier, Amsterdam.

Aiuppa, A., and C. Federico (2004), Anomalous magmatic degassing prior to the 5th April 2003 paroxysm on Stromboli, *Geophys. Res. Lett.*, *31*, L14607, doi:10.1029/2004GL020458.

Allard, P. (2009), A CO_2-rich gas trigger of explosive paroxysms at Stromboli basaltic volcano, Italy, *J. Volcanol. Geotherm. Res.*, *189*, 363–374.

Allard, P., P. Baxter, M. Halbwachs, and J.-C. Komorowski (2002), The January 2002 eruption of Nyiragongo Volcano (Dem. Repub. Congo) and related hazards: Observations and recommendations, Final Report of the French-British Scientific Team: submitted to the Ministry of Foreign Affairs, Paris, France, Foreign Office, London, United Kingdom, and respective embassies in Democratic Republic of Congo and Republic of Rwanda, pp. 1–24.

Amelung, F., S. Jónsson, H. Zebker, and P. Segall (2000), Widespread uplift and "trapdoor" faulting on Galápagos volcanoes observed with radar interferometry, *Nature*, *407*, 993–996.

Amma-Miyasaka, M., M. Nakagawa, and S. Nakada (2005), Magma plumbing system of the 2000 eruption of Miyakejima Volcano, Japan, *Bull. Volcanol.*, *67*, 254–267, doi:10.1007/s00445-004-0408-0.

Arellano, S. R., M. Mall, P. Samaniego, J.-L. Le Pennec, A. Ruiz, I. Molina, and H. Yepes (2008), Degassing patterns of Tungurahua volcano (Ecuador) during the 1999–2006 eruptive period, inferring from remote spectroscopic measurements of SO_2 emissions, *J. Volcanol. Geotherm. Res.*, *176*, 151–162, doi:10.1016/j.jvolgeores.208.07.007.

Arvidsson, R., and G. Ekström (1998), Global CMT analysis of moderate earthquakes, $M_W \geq 4.5$, using intermediate-period surface waves, *Bull. Seismol. Soc. Am.*, *88*(4), 1003–1013.

Bai, C.-Y., and S. Greenhalgh (2005), 3D multi-step travel time tomography: Imaging the local, deep velocity structure of Rabaul volcano, Papua New Guinea, *Phys. Earth Planet. Inter.*, *151*, 259–275.

Bailey, D. K. (1993), Carbonate magmas, *J. Geolog. Soc. London*, *150*, 637–651, doi:10.1144/gsjgs.150.4.0637.

Barba, D., S. Arellano, P. Ramon, P. Mothes, A. Alvarado, G. Ruiz, and L. Troncoso (2006), Cronologia de los Eventos Eruptivos de Julio y Agosto del 2006 del Volcan Tungurahua, Resumenes extendidos de las 6th Jornadas en Ciencias de la Tierra, EPN-DG, Quito, Ecuador, pp. 177–180.

Bassin, C., G. Laske, and G. Masters (2000), The current limits of resolution for surface wave tomography in North America, *Eos Trans. AGU*, *81*(48), Fall. Meet. Suppl., Abstract T31B-1820.

Bertagnini, A., N. Métrich, P. Landi, and M. Rosi (2003), Stromboli volcano (Aeolian Archipelago, Italy): An open window on the deep-feeding system of a steady state basaltic volcano, *J. Geophys. Res.*, *108*(B7), 2336, doi:10.1029/2002JB002146.

Bird, P. (2003), An updated digital model of plate boundaries, *Geochem. Geophys. Geosyst.*, *4*(3), doi:10.1029/2001GC000252.

Calder, E. S., R. Luckett, R. S. J. Sparks, and B. Voight (2002), Mechanisms of lava dome instability and generation of rockfalls and pyroclastic flows at Soufrière Hills Volcano, Montserrat, in *The Eruption of Soufrière Hills Volcano, Montserrat, from 1995 to 1999*, edited by T. H. Druitt and B. P. Kokelaar, pp. 173–190, Geological Society, London.

Calvari, S., L. Spampinato, and L. Lodato (2006), The 5 April 2003 vulcanian paroxysmal explosion at Stromboli volcano (Italy) from field observations and thermal data, *J. Volcanol. Geotherm. Res.*, *149*, 160–175.

Caplan-Auerbach, J., and F. K. Duennebier (2001), Seismicity and velocity structure of Loihi Seamount from the 1996 earthquake swarm, *Bull. Seismol. Soc. Am.*, *91*(2), 178–190.

Carapezza, M. L., S. Inguaggiato, L. Brusca, and M. Longo (2004), Geochemical precursors of the activity of an open-conduit volcano: The Stromboli 2002–2003 eruptive events, *Geophys. Res. Lett.*, *31*, L07620, doi:10.1029/2004GL019614.

Carn, S. A., A. J. Kruegger, N. A. Krotkov, S. Arellano, and K. Yang (2008), Daily monitoring of Ecuadorian volcanic degassing from space, *J. Volcanol. Geotherm. Res.*, *176*(1), 151–162.

Cesca, S., T. Braun, E. Tessmer, and T. Dahm (2007), Modelling of the April 5, 2003, Stromboli (Italy) paroxysmal eruption from the inversion of broadband seismic data, *Earth Planet. Sci. Lett.*, *261*, 164–178.

Chadwick, W. W., D. J. Geist, S. Jónsson, M. Poland, D. J. Johnson, and C. M. Meertens (2006), A volcano bursting at the seams: Inflating, faulting, and eruption at Sierra Negra volcano, Galápagos, *Geology*, *34*(12), 1025–1028, doi:10.1130/G22826A.1.

Chadwick, W. W., K. V. Cashman, R. W. Embley, H. Matsumoto, R. P. Dziak, C. E. J. de Ronde, T. K. Lau, N. D. Deardorff, and S. G. Merle (2008), Direct video and hydrophone observations of submarine explosive eruptions at NW Rota-1 volcano, Mariana arc, *J. Geophys. Res.*, *113*, B08S10, doi:10.1029/2007JB005215.

Chadwick, W. W., R. P. Dziak, J. H. Haxel, R. W. Embley, and H. Matsumoto (2012), Submarine landslide triggered by volcanic eruption recorded by in situ hydrophone, *Geology*, *40*(1), doi:10.1130/G32495.1.

Cole, J. W., D. M. Milner, and K. D. Spinks (2005), Calderas and caldera structures: A review, *Earth-Sci. Rev.*, *69*, 1–26.

D'Auria, L., F. Giudicepietro, M. Martini, and R. Peluso (2006), Seismological insights into the kinematics of the 5 April 2003 vulcanian explosion at Stromboli volcano (southern Italy), *Geophys. Res. Lett.*, *33*, L08308, doi:10.1029/2006GL026018.

Davis, A. S., and D. A. Clague (1998), Changes in the hydrothermal system at Loihi Seamount after the formation of Pele's pit in 1996, *Geology*, *26*(5), 399–402.

de Bromand d'Ars, J., C. Jaupart, and R. S. J. Sparks (1995), Distribution of volcanoes in active margins, *J. Geophys. Res.*, *100*(B10), 20,421–20,432, doi:10.1029/95JB02153.

De Natale, G., and F. Pingue (1993), Ground deformations in collapsed caldera structures, *J. Volanol. Geotherm. Res.*, *57*, 19–38.

Demant, A., P. Lestrade, R. T. Lubala, A. B. Kampunzu, and J. Durieux (1994), Volcanological and petrological evolution of Nyiragongo volcano, Virunga volcanic field, Zaire, *Bull. Volcanol.*, *56*, 47–61.

Doyle, A. C., R. J. Singleton, and J. C. Yaldwyn (1979), Volcanic activity and recent uplift on Curtis and Cheeseman Islands, Kermadec Group, Southwest Pacific, *J. Royal Soc. New Zealand*, *9*(1), 123–140.

Dreger, D. S., H. Tkalčić, and M. Johnston (2000), Dilatational processes accompanying earthquakes in the Long Valley caldera, *Science*, *228*(122), doi:10.1126/science.288.5463.122.

Druitt, T. H., E. S. Calder, P. D. Cole, R. P. Hoblitt, S. C. Loughlin, G. E. Norton, L. J. Ritchie, R. S. J. Sparks, and B. Voight (2002), Small-volume, highly mobile pyroclastic flows formed by rapid sedimentation from pyroclastic surges at Soufrière Hills Volcano, Montserrat: An important volcanic hazard, in *The Eruption of Soufrière Hills Volcano, Montserrat, from 1995 to 1999*, edited by T. H. Druitt and B. P. Kokelaar, pp. 263–279, Geological Society, London.

Duennebier, F. K., et al. (1997), Researchers rapidly respond to submarine activity at Loihi volcano, *Hawaii, Eos, Trans. AGU*, *78*(22), 229–233.

Dufumier, H., and L. Rivera (1997), On the resolution of the isotropic component in moment tensor inversion, *Geophys. J. Int.*, *131*, 595–606.

Dziewonski, A. M., and D. L. Anderson (1981), Preliminary reference Earth model, *Phys. Earth Planet. Inter.*, *25*(4), 297–356.

Dziewonski, A. M., and J. H. Woodhouse (1983), An experiment in systematic study of global seismicity: Centroid-moment tensor solutions for 201 moderate and large earthquakes of 1981, *J. Geophys. Res.*, *88*(B4), doi:10.1029/JB088iB04p03247.

Dziewonski, A. M., T.-A. Chou, and J. H. Woodhouse (1981), Determination of earthquake source parameters from waveform data for studies of global and regional seismicity, *J. Geophys. Res.*, *86*(B4), 2825–2852.

Dziewonski, A. M., A. Friedman, D. Giardini, and J. H. Woodhouse (1983), Global seismicity of 1982: Centroid-moment tensor solutions for 308 earthquakes, *Phys. Earth Planet. Inter.*, *33*, 76–90.

Dziewonski A. M., J. E. Franzen, and J. H. Woodhouse (1984), Centroid-moment tensor solutions for January–March 1984, *Phys. Earth Planet. Inter*, *34*, 209–219.

Dziewonski, A. M., G. Ekström, and M. Nettles (1997), Harvard centroid-moment tensor solutions 1976–96: Significance of the non-double-couple component, in *Rockbursts and Seismicity in Mines*, edited by S. J. Gibowicz and S. Lasocki, pp. 3–16, A. A. Balkema, Brookfield, VT.

Ekström, G. (1989), A very broad band inversion method for the recovery of earthquake source parameters, *Tectonophysics*, *166*, 73–100.

Ekström, G. (1994), Anomalous earthquakes on volcano ring-fault structures, *Earth Planet. Sci. Lett.*, *128*, 707–712.

Ekström, G. (2006), Global detection and location of seismic sources by using surface waves, *Bull. Seismol. Soc. Am.*, *96*(4A), 1201–1212, doi:10.1785/0120050175.

Ekström, G., and M. Nettles (2002), Detection and location of slow seismic sources using surface waves, *Eos Trans. AGU*, *83*(47), Fall Meet. Suppl., Abstract S72E-06.

Ekström, G., J. Tromp, and E. W. F. Larson (1997), Measurements and global models of surface wave propagation, *J. Geophys. Res.*, *102*, 8137–8157.

Ekström, G., A. Dziewonski, N. Maternovskaya, and M. Nettles (2005), Global seismicity of 2003: Centroid-moment-tensor solutions for 1087 earthquakes, *Phys. Earth Planet. Inter.*, *148*(2-4), 327–351, doi:10.1016/j.pepi.2004.09.006.

Ekström, G., M. Nettles, and A. M. Dziewonski (2012), The Global CMT project 2004–2010: Centroid-moment tensors for 13,017 earthquakes, *Phys. Earth Planet. Inter.*, *200-201*, 1–9, doi:10.1016.j.pepi.2012.04.002.

Embley, R. W., et al. (2006), Long-term eruptive activity at a submarine arc volcano, *Nature*, *441*, 494–497, doi:10.1038/nature04762.

Fee, D., M. Garces, and A. Steffke (2010), Infrasound from Tungurahua Volcano 2006-2008: Strombolian to plinian eruptive activity, *J. Volcanol. Geotherm. Res.*, *193*, 67–81, doi:10.1016/j.jvolgeores.2010.03.006.

Finlayson, D. M., O. Gudmundsson, I. Itikarai, Y. Nishimura, and H. Shimamura (2003), Rabaul volcano, Papua New Guinea: Seismic tomographic imaging of an active caldera, *J. Volcanol. Geotherm. Res.*, *124*, 153–171.

Fichtner, A., and H. Tkalčić (2010), Insights into the kinematics of a volcanic caldera drop: Probabilistic finite-source inversion of the 1996 Bárdarbunga, Iceland, earthquake, *Earth Planet. Sci. Lett.*, *297*, 607–615, doi:10.1016/j.epsl.2010.07.013.

Foulger, G. R., and B. R. Julian (1993), Non-double-couple earthquakes at the Hengill-Grensdalur Volcanic Complex, Iceland: Are they artifacts of crustal heterogeneity? *Bull. Seism. Soc. Am.*, *83*(1), 38–52.

Foulger, G. R., B. R. Julian, D. P. Hill, A. M. Pitt, P. E. Malin, and E. Shalev (2004), Non-double-couple microearthquakes at Long Valley caldera, California, provide evidence for hydraulic fracturing, *J. Volcanol. Geotherm. Res.*, *132*, 45–71.

Francalanci, L., A. Bertagnini, N. Métrich, A. Renzulli, R. Vannucci, P. Landi, S. Del Moro, M. Menna, C. M. Petrone, and I. Nardini (2008), Mineralogical, geochemical, and isotopic characteristics of the ejecta from the 5 April 2003 paroxysm at Stromboli, Italy: Inferences on the preeruptive magma dynamics, in *The Stromboli Volcano: An Integrated Study of the 2002–2003 Eruption*, edited by S. Calvari, et al., pp. 331–345, AGU, Washington, D. C.

Frohlich, C. (1989), Note concerning possible mechanisms for non-double-couple earthquake sources, *Geophys. Res. Lett.*, *16*(6), 523–526.

Frohlich, C. (1990a), Earthquakes with non-double-couple mechanisms, *Science*, *264*, 804–809.

Frohlich, C. (1990b), Note concerning non-double-couple source components from slip along surfaces of revolution, *J. Geophys. Res.*, *95*(B5), 6861–6866.

Frohlich, C. (1995), Characteristics of well-determined non-double-couple earthquakes in the Harvard CMT catalog, *Phys. Earth Planet. Inter.*, *21*(4), 213–228, doi:10.1016/0031-9201(95)03031-Q.

Fujita, E., M. Ukawa, E. Yamamoto, Y. Okada, and M. Kikuchi (2001), Volcanic earthquakes and tremors associated with the 2000 Miyakejima Volcano eruption (in Japanese with English abstract), *J. Geogr.*, *110*(2), 191–203.

Fujita, E., M. Ukawa, E. Yamamoto, and Y. Okada (2002), Cyclic jerky opening of magma sheet and caldera formation during the 2000 Miyakejima volcano eruption, *Geophys. Res. Lett.*, *29*(9), 1326, doi:10.1029/2001GL013848.

Fujita, E., M. Ukawa, and E. Yamamoto (2004), Subsurface cyclic magma sill expansions in the 2000 Miyakejima volcano eruption: Possibility of two-phase flow oscillation, *J. Geophys. Res.*, *109*, B04205, doi:10.1029/2003JB002556.

Furuya, M., S. Okubo, W. Sun, Y. Tanaka, J. Oikawa, and H. Watanabe (2003), Spatiotemporal gravity changes at Miyakejima Volcano, Japan: Caldera collapse, explosive eruptions and magma movement, *J. Geophys. Res.*, *108*(B4), 2219, doi:10.1029/2002JB001989.

Garcia, M. O., K. H. Rubin, M. D. Norman, J. M. Rhodes, D. W. Graham, D. W. Muenow, and K. Spencer (1998), Petrology and geochronology of basalt breccia from the 1996 earthquake swarm of Loihi seamount, Hawaii: Magmatic history of its 1996 eruption, *Bull. Volcanol.*, *59*, 577–592.

Garcia, M. O., J. Caplan-Auerbach, E. H. De Carlo, M. D. Kurz, and N. Becker (2006), Geology, geochemistry and earthquake history of Loihi Seamount, Hawaii's youngest volcano, *Chemie der Erde*, *66*, 81–108.

Geist, D. J., K. S. Harpp, T. R. Naumann, M. Poland, W. W. Chadwick, M. Hall, and E. Rader (2008), The 2005 eruption of Sierra Negra volcano, Galápagos, Ecuador, *Bull. Volcanol.*, *70*, 655–673, doi:10.1007/s00445-007-0160-3.

Geshi, N. (2009), Asymmetric growth of collapsed caldera by oblique subsidence during the 2000 eruption of Miyakejima, Japan, *Earth Planet. Sci. Lett.*, *280*, 149–158.

Geshi, N., and T. Oikawa (2008), Phreatomagmatic eruptions associated with the caldera collapse during the Miyakejima 2000 eruption, Japan, *J. Volcanol. Geotherm. Res.*, *176*, 457–468.

Geshi, N., T. Shimano, T. Chiba, and S. Nakada (2002), Caldera collapse during the 2000 eruption of Miyakejima Volcano, Japan, *Bull. Volcanol.*, *64*, 55–68, doi:10.1007/s00445-001-0184-z.

Geyer, A., and J. Gottsman (2010), The influence of mechanical stiffness on caldera deformation and implications for the 1971–1984 Rabaul uplift (Papua New Guinea), *Tectonophysics*, *483*, 399–412.

Gudmundsson, M. T., F. Sigmundsson, and H. Björnsson (1997), Ice-volcano interaction of the 1996 Gjálp subglacial eruption, Vatnajökull, Iceland, *Nature*, *389*, 954–957, doi:10.1038/40122.

Gudmundsson, A. (2008), Magma-chamber geometry, fluid transport, local stresses and rock behavior during collapse caldera formation, in *Caldera Volcanism: Analysis, Modelling and Response*, *Developments in Volcanology*, vol. 10, edited by J. Gottsman and J. Marti, pp. 313–349, Elsevier, Amsterdam.

Hall, M. L., C. Robin, B. Beate, P. Mothes, and M. Monzier (1999), Tungurahua Volcano, Ecuador: Structure, eruptive history and hazards, *J. Volcanol. Geotherm. Res.*, *91*, 1–21.

Hanson, J. B., Y. Lavallée, F. Goldstein, U. Kueppers, K.-U. Hess, and D. Dingwell (2011), A rheological map of Tungurahua Volcano (Ecuador): Explaining the explosive-effusive transition, paper presented at Fragile Earth: Geological Processes from Global to Local Scales and Associated Hazards, München, Germany.

Harlow, D. H., J. A. Power, E. P. Laguerta, G. Ambubuyog, R. A. White, and R. P. Hoblitt (1996), Precursory seismicity and forecasting of the June 15, 1991 eruption of Mount Pinatubo, in *Fire and Mud: Eruptions and Lahars of Mount Pinatubo, Philippines*, edited by C. G. Newhall and R. S. Punongbayan, pp. 285–306, Univ. of Washington Press, Seattle.

Harris, A. J. L., M. Ripepe, S. Calvari, L. Lodato, and L. Spampinato (2008), The 5 April 2003 explosion of Stromboli: Timing of eruption dynamics using thermal data, in *The Stromboli Volcano: An Integrated Study of the 2002–2003 Eruption*, edited by S. Calvari, et al., pp. 306–316, AGU, Washington, D.C.

Hart, S. R., et al. (2000), Vailulu'u undersea volcano: The new Samoa, *Geochem. Geophys. Geosys.*, *8*(1), doi:10.1029/2000GC000108.

Harvey, D., and G. L. Choy (1982), Broad-band deconvolution of GDSN data, *Geophys. J. R. Astron. Soc.*, *69*(3), 659–668.

Heeszel, D. S., D. A. Wiens, P. J. Shore, H. Shiobara, and H. Sugioka (2008), Earthquake evidence for along-arc extension in the Mariana Islands, *Geochem. Geophys. Geosys.*, *9*(12), Q12X03, doi:10.1029/2008GC002186.

Hjörleifsdóttir, V., and G. Ekström (2010), Effects of three-dimensional Earth structure on CMT earthquake parameters, *Phys. Earth Planet. Inter.*, *179*, 178–190.

Hoblitt, R. P., E. W. Wolfe, W. E. Scott, M. R. Couchman, J. S. Pallister, and D. Javier (1996), The preclimactic eruptions of Mount Pinatubo, June 1991, in *Fire and Mud: Eruptions and Lahars of Mount Pinatubo, Philippines*, edited by C. G. Newhall and R. S. Punongbayan, pp. 457–511, Univ. of Washington Press, Seattle.

Iguchi, M., K. Yamamoto, T. Takayama, T. Maekawa, T. Nishimura, H. Hashino, H. Yakihara, and S. Hirano (2001), Characteristics of volcanic earthquakes at Kuchierabujima volcano. Geophysical and Geochemical Joint Observation of 2000 (in Japanese with English abstract), *Disaster Prev. Res. Inst., Kyoto Univ.*, *44B-1*, 317–326.

Isacks, B, J. Oliver, and L. R. Sykes (1968), Seismology and the new global tectonics, *J. Geophys. Res.*, *73*(18), 5855–5899, doi:10.1029/JB073i018p05855.

Itikarai, I. (2008), The 3-D structure and earthquake locations at Rabaul Caldera, Papua New Guinea. Unpublished Master of Philosophy thesis, Australian National University, Canberra, 137 pp.

Ito, T., and S. Yoshioka (2002), A dike intrusion model in and around Miyakejima, Niijima and Kozushima in 2000, *Tectonophysics*, *359*, 171–187.

Johnson, R. W., I. Itikarai, H. Patia, and C. O. McKee (2010), Volcanic systems of the Northeastern Gazelle Peninsula, Papua New Guinea: Synopsis, evaluation, and a model for Rabaul Volcano, Papua New Guinea, *Rabaul Volcano Workshop Report*, Papua New Guinea Department of Mineral Policy and Geohazards Management, and Australian Agency for International Development, Port Moresby, Papua New Guinea.

Jones, R. H., and R. C. Stewart (1997), A method for determining significant structures in a cloud of earthquakes, *J. Geophys. Res.*, *102*(B4), 8245–8254.

Jónsson, S., H. Zebker, and F. Amelung (2005), On trapdoor faulting at Sierra Negra volcano, Galápagos, *J. Volcanol. Geotherm. Res.*, *144*, 59–71.

Jónsson, S. (2009), Stress interaction between magma accumulation and trapdoor faulting on Sierra Negra, Galápagos, *Tectonophysics*, *471*, 36–44.

Julian, B. R. (1983), Evidence for dyke intrusion earthquake mechanisms near Long Valley caldera, California, *Nature*, *303*, 323–325, doi:10.1038/303323a0.

Julian, B. R., and S. A. Sipkin (1985), Earthquake processes in the Long Valley caldera area, California, *J. Geophys. Res.*, *90*(B13), 11,155–11,169, doi:10.1029/JB090iB13p11155.

Julian, B. R., A. D. Miller, and G. R. Foulger (1998), Non-double-couple earthquakes 1. Theory, *Rev. Geophys.*, *36*(4), 525–549.

Kanamori, H., G. Ekström, A. Dziewonski, J. S. Barker, and S. A. Sipkin (1993), Seismic radiation by magma injection: An anomalous seismic event near Tori Shima, Japan, *J. Geophys. Res.*, *98*(B4), 6511–6522.

Kaneko, T., A. Yasuda, T. Shimano, S. Nakada, T. Fujii, T. Kanazawa, A. Nishizawa, and Y. Matsumoto (2005), Submarine flank eruption preceding caldera subsidence during the 2000 eruption of Miyakejima Volcano, Japan, *Bull. Volcanol.*, *67*, 243–253, doi:10.1007/s00445-004-0407-1.

Kawakatsu, H. (1996), Observability of the isotropic component of a moment tensor, *Geophys. J. Int.*, *126*, 525–544.

Kazahaya, K., H. Shinohara, K. Uto, M. Odai, Y. Nakahori, H. Mori, H. Iino, M. Miyashita, and J. Hirabayashi (2004), Gigantic SO_2 emission from Miyakejima volcano, Japan, caused by caldera collapse, *Geology*, *32*(5), 425–428, doi:10.1130/G20399.1.

Kikuchi, M., Y. Yamanaka, and K. Koketsu (2001), Source Process of the Long-period Seismic Pulses Associated with the 2000 Eruption of Miyake-jima Volcano, and its Implications (in Japanese with English abstract), *J. Geogr.*, *110*(2), 204–216.

Knopoff, L., and M. J. Randall (1970), The compensated linear-vector dipole: A possible mechanism for deep earthquakes, *J. Geophys. Res.*, *75*(26), 4957–4963.

Kobayashi, T., T. Ohminato, and Y. Ida (2003), Earthquake series preceding very long period seismic signals, observed during the 2000 Miyake-jima volcanic activity, *Geophys. Res. Lett.*, *30*(8), 1423, doi:10.1029/2002GL016631.

Komorowski, J.-C., et al. (2002/2003), The January 2002 flank eruption of Nyiragongo Volcano (Democratic Republic of Congo): Chronology, evidence for a tectonic rift trigger, and impact of lava flows on the City of Goma, *Acta Vulcanol.*, *14/15*(1–2), 27–62.

Konstantinou, K. I., H. Kao, C. H. Lin, and W.-T. Liang (2003), Analysis of broad-band regional waveforms of the 1996 September 29 earthquake at Bárdarbunga volcano, central Iceland: investigation of the magma injection hypothesis, *Geophys. J. Int.*, *154*, 134–145.

Konter, J. G., H. Staudigel, S. R. Hart, and P. M. Shearer (2004), Seafloor seismic monitoring of an active submarine volcano: Local seismicity at Vailulu'u Seamount, Samoa, *Geochem. Geophys. Geosyst.*, *5*(6), doi:10.1029/2004GC000702.

Kumagai, H., T. Ohminato, M. Nakano, M. Ooi, A. Kubo, H. Inoue, and J. Oikawa (2001), Very-long-period seismic signals and caldera formation at Miyake Island, Japan, *Science*, *293*(5530), 687–690.

Kumagai, H., B. A. Chouet, and P. B. Dawson (2005), Source process of along-period event at Kilauea volcano, Hawaii, *Geophys. J. Int.*, *161*, 243–254.

Kumagai, H., et al. (2007a), Enhancing volcano-monitoring capabilities in Ecuador, *Eos, Trans. AGU*, *88*(23), 245, doi:10.1029/2007EO230001.

Kumagai, H., H. Yepes, M. Nakano, and I. Molina (2007b), Very-long-period signals observed immediately before a Vulcanian eruption accompanying pyroclastic flows at Tungurahua, Ecuador, paper presented at Japan Geoscience Union Meeting, Chiba City, Japan.

Kumagai, H., M. Nakano, T. Maeda, H. Yepes, P. Palacios, M. Ruiz, S. Arrais, M. Vaca, I. Molina, and T. Yamashima (2010), Broadband seismic monitoring of active volcanoes using deterministic and stochastic approaches, *J. Geophys. Res.*, *115*, B08303, doi:10.1029/2009JB006889.

LeMasurier, W. E., J. Thomson, P. Baker, P. Kyle, P. Rowley, J. Smellie, and W. Verwoerd (Eds.) (1990), *Volcanoes of the Antarctic Plate and Southern Oceans*, *Antarctic Res. Ser.*, *48*, 487 pp., AGU, Washington, D. C., doi:10.1029/AR048.

Lynch, J. S., and G. Stephens (1996), Mount Pinatubo: A satellite perspective of the June 1991 eruptions, in *Fire and Mud: Eruptions and Lahars of Mount Pinatubo, Philippines*, edited by C. G. Newhall and R. S. Punongbayan, pp. 637–645, Univ. of Washington Press, Seattle.

Marti, J., A. Geyer, A. Folch, and J. Gottsman (2008), A review on collapse caldera modelling, in *Caldera Volcanism: Analysis, Modelling and Response*, *Developments in Volcanology*, vol. 10, edited by J. Gottsman and J. Marti, pp. 233–283, Elsevier, Amsterdam.

Matoza, R. S., D. Fee, M. A. Garcés, J. M. Seiner, P. A. Ramón, and M. A. H. Hedlin (2009), Infrasonic jet noise from volcanic eruptions, *Geophys. Res. Lett.*, *36*, L08303, doi:10.1029/2008GL036486.

McKee, C. O., P. L. Lowenstein, P. de Saint Ours, B. Talai, I. Itikarai, and J. J. Mori (1984), Seismic and ground deformation crises at Rabaul caldera: Prelude to an eruption?, *Bull. Volcanol.*, *47*(2), 397–411.

Métrich, N., A. Bertagnini, P. Landi, M. Rosi, and O. Belhadj (2005), Triggering mechanism at the origin of paroxysms at Stromboli (Aeolian Archipelago, Italy): The 5 April 2003 eruption, *Geophys. Res. Lett.*, *32*, L10305, doi:10.1029/2004GL022257.

Michon, L., N. Villeneuve, T. Catry, and O. Merle (2009), How summit calderas collapse on basaltic volcanoes: New insights from the April 2007 caldera collapse of Piton de la Fournaise volcano, *J. Volcanol. Geotherm. Res.*, *184*, 138–151.

Michon, L., F. Massin, V. Famin, V. Ferrazzini, and G. Roult (2011), Basaltic calderas: Collapse dynamics, edifice deformation, and variations of magma withdrawal., *J. Geophys. Res.*, *116*, B03209, doi:10.1029/2010JB007636.

Miller, A. D., G. R. Foulger, and B. R. Julian (1998a), Non-double-couple earthquakes 2. Observations, *Rev. Geophys.*, *36*(4), 551–568.

Miller, A. D., B. R. Julian, and G. R. Foulger (1998b), Three-dimensional seismic structure and moment tensors of non-double-couple earthquakes at the Hengill-Grensdalur volcanic complex, Iceland, *Geophys. J. Int.*, *133*, 309–325.

Minson, S. E., and D. S. Dreger (2008), Stable inversions for complete moment tensors, *Geophys. J. Int.*, *174*, 585–592.

Minson, S. E., D. S. Dreger, R. Bürgmann, H. Kanamori, and K. M. Larson (2007), Seismically and geoetically determined nondouble-couple source mechanisms from the 2000 Miyakejima volcanic earthquake swarm, *J. Geophys. Res.*, *112*, B10308, doi:10.1029/2006JB004847.

Moran, S. C., C. Newhall, and D. C. Roman (2011), Failed magmatic eruptions: Late-stage cessation of magma ascent, *Bull. Volcanol.*, *73*, 115–122, doi:10.1007/s00445-010-0444-x.

Mori, J., and C. McKee (1987), Outward-dipping ring-fault structure at Rabaul caldera as shown by earthquake locations, *Science*, *235*, 193–195.

Mori, J., C. McKee, I. Itikarai, P. Lowenstein, P. de Saint Ours, and B. Talai (1989), Earthquakes of the Rabaul seismo-deformational crisis September 1983 to July 1985 seismicity on a ring fault. in *Volcanic Hazards: Assessment and Monitoring, IAVCEI Proceedings in Volcanology*, edited by J. H. Latter, pp. 429–462, Springer.

Mori, J., R. A. White, D. H. Harlow, P. Okubo, J. A. Power, R. P. Hoblitt, E. P. Laguerta, A. Lanzuza, and B. C. Bautista (1996), Volcanic earthquakes following the 1991 climactic eruption of Mount Pinatubo: Strong seismicity during a waning eruption, in *Fire and Mud: Eruptions and Lahars of Mount Pinatubo, Philippines*, edited by C. G. Newhall and R. S. Punongbayan, pp.339–350, Univ. of Washington Press, Seattle.

Murase, M., et al. (2006), Time dependent model of magma intrusion in and around Miyake and Kozu Islands, Central Japan in June–August, 2000, *J. Volcanol. Geotherm. Res.*, *150*, 213–231.

Nairn, I. A., C. O. McKee, B. Talai, and C. P. Wood (1995), Geology and eruptive history of the Rabaul caldera area, Papua New Guinea, *J. Volcanol. Geotherm. Res.*, *69*(3–4), 255–284.

Nakada, S., M. Nagai, T. Kaneko, A. Nozawa, and K. Suzuki-Kamata (2005), Chronology and products of the 2000 eruption of Miyakejima Volcano, Japan, *Bull. Volcanol.*, *67*, 205–218, doi:10.1007/s00445-004-0404-4.

Nakanishi, I., and H. Kanamori (1982), Effects of lateral heterogeneity and source process time on the linear moment tensor inversion of long-period Rayleigh-waves, *Bull. Seism. Soc. Am.*, *72*(6), 2063–2080.

Nakano, M., and H. Kumagai (2005), Waveform inversion of volcano-seismic signals assuming possible source geometries, *Geophys. Res. Lett.*, *31*, L12302, doi:10.1029/2005GL022666.

Nettles, M., and G. Ekström (1998), Faulting mechanism of anomalous earthquakes near Bárdarbunga Volcano, Iceland, *J. Geophys. Res.*, *103*(B8), 17,973–17,983.

Newhall, C. G., and S. Self (1982), The Volcanic Explosivity Index (VEI): An estimate of explosive magnitude for historical volcanism, *J. Geophys. Res.*, *87*(C2), 1231–1238.

Nishimura, T., S. Ozawa, M. Murakami, T. Sagiya, T. Tada, M. Kaidzu, and M. Ukawa (2001), Crustal deformation caused by magma migration in the northern Izu Islands, Japan, *Geophys. Res. Lett.*, *28*(19), 3745–3748.

Ohminato, T. (2008), Source mechanisms of vulcanian eruptions at Mt. Asama, Japan, inferred from volcano seismic signals, *Geol. Soc. London, Special Pub. 2008*, *307*, 189–206, doi:10.1144/SP307.11.

Ohminato, T., and H. Kumagai (2001), On the very-long-period seismic pulses observed during the 2000 Miyake-jima volcanic activity (in Japanese with English abstract), paper presented at Volcanic Structure in the Shallow Part and Volcanic Fluid, Disaster Prevention Research Institute, Kyoto University, available at http://www.dpri.kyoto-u.ac.jp/~kazan/12k03/ohminato.pdf.

Ohminato, T., B. A. Chouet, P. Dawson, and S. Kedar (1998), Waveform inversion of very long period impulsive signals associated with magmatic injection beneath Kilauea Volcano, Hawaii, *J. Geophys. Res.*, *103*(B10), 23,839–23,862.

Ohminato, T., M. Takeo, H. Kumagai, T. Yamashina, J. Oikawa, E. Koyama, H. Tsuji, and T. Urabe (2006), Vulcanian eruptions with dominant single force components observed during the Asama 2004 volcanic activity in Japan, *Earth Planets Space*, *58*, 583–593.

Oppenheimer, C. (1998), Satellite observation of active carbonatite volcanism at Ol Doinyo Lengai, Tanzania, *Int. J. Remote Sensing*, *19*(1), 55–64.

Ozawa, S., S. Miyazaki, T. Nishimura, M. Murakami, M. Kaidzu, T. Imakiire, and X. Ji (2004), Creep, dike intrusion, and magma chamber deflation model for the 2000 Miyake eruption and the Izu islands earthquakes, *J. Geophys. Res.*, *109*, B02410, doi:10.1029/2003JB002601.

Power, J. A., T. L. Murray, J. N. Marso, and E. P. Laguerta (1996), Preliminary observations of seismicity at Mount Pinatubo by use of the Seismic Spectral Amplitude Measurement (SSAM) System, May 13–June 18, 1991, in *Fire and Mud: Eruptions and Lahars of Mount Pinatubo, Philippines*, edited by C. G. Newhall and R. S. Punongbayan, pp. 269–284, Univ. of Washington Press, Seattle.

Reynolds, R. W., D. Geist, and M. D. Kurz (1995), Physical volcanology and structural development of Sierra Negra volcano, Isabela Island, Galápagos archipelago, *Geol. Soc. Am. Bull.*, *107*(12), 1398–1410, doi:10.1130/0016-7606(1995)107<1398:PVASDO>2.3.CO;2.

Ripepe, M., and A. J. L. Harris (2008), Dynamics of the 5 April 2003 explosive paroxysm observed at Stromboli by a near-vent thermal, seismic and infrasonic array, *Geophys. Res. Lett.*, *35*, L07306, doi:10.1029/2007GL032533.

Ritchie, L. J., P. D. Cole, and R. S. J. Sparks (2002), Sedimentology of deposits from the pyroclastic density current of 26 December 1997 at Soufrière Hills Volcano, Montserrat, in *The Eruption of Soufrière Hills Volcano, Montserrat, from 1995 to 1999*, edited by T. H. Druitt and B. P. Kokelaar, pp. 435–456, Geological Society, London.

Rizzo, A., A. Aiuppa, G. Capasso, F. Grassa, S. Inguaggiato, M. Longo, and M. L. Carapezza (2008), The 5 April 2003 paroxysm at Stromboli: A review of geochemical observations, in *The Stromboli Volcano: An Integrated Study of the 2002–2003 Eruption*, edited by S. Calvari, et al., pp. 347–358, AGU, Washington, D. C.

Rosi, M., A. Bertagnini, A. J. L. Harris, L. Pioli, M. Pistolesi, and M. Ripepe (2006), A case history of paroxysmal explosion at Stromboli: Timing and dynamics of the April 5, 2003 event, *Earth Planet. Sci. Lett.*, *243*, 594–606.

Ross, A., G. R. Foulger, and B. R. Julian (1996), Non-double-couple earthquake mechanisms at the Geysers geothermal area, California, *Geophys. Res. Lett.*, *23*, 877–880.

Rouland, D., C. Condis, C. Parmentier, and A. Souriau (1992), Previously undetected earthquakes in the southern hemisphere located using long-period Geoscope data, *Bull. Seism. Soc. Am.*, *82*(6), 2448–2463.

Ryan, W. B. F., et al. (2009), Global multi-resolution topography synthesis, *Geochem. Geophys. Geosys.*, *10*(3), doi:10.1029/2008GC002332.

Sahama, T. G. (1973), Evolution of the Nyiragongo magma, *J. Petrolog.*, *14*(1), 33–48.

Saito, G., K. Uto, K. Kazahaya, H. Shinohara, Y. Kawanabe, and H. Satoh (2005), Petrological characteristics and volatile content of magma from the 2000 eruption of Miyakejima Volcano, Japan, *Bull. Volcanol.*, *67*, 268–280, doi:10.1007/s00445-004-0409-z.

Sakai, S., T. Yamada, S. Ide, M. Mochizuki, H. Shiobara, T. Urabe, N. Hirata, M. Shinohara, T. Kanazawa, A. Nishizawa, G. Fujie, and H. Mikada (2001), Magma migration from the point of view of seismic activity in the volcanism of Miyake-jima Island in 2000 (in Japanese with English abstract), *J. Geogr.*, *110*(2), 145–155.

Samaniego, P., J.-L. Le Pennec, C. Robin, and S. Hidalgo (2011), Petrological analysis of the pre-eruptive magmatic process prior to the 2006 explosive eruptions at Tungurahua volcano (Ecuador), *J. Volcanol. Geotherm. Res.*, *199*, 69–84, doi:10.1016/j.jvolgeores.2010.10.010.

Sasai, Y., M. Uyeshima, H. Utada, T. Kagiyama, J. Zlotnicki, T. Hashimoto, and Y. Takahashi (2001), The 2000 activity of Miyake-jima Volcano as Inferred from electric and magnetic field observations, *J. Geogr.*, *110*(2), 226–244.

Sasai, Y., M. Uyeshima, J. Zlotnicki, H. Utada, T. Kagiyama, T. Hashimoto, and Y. Takahashi (2002), Magnetic and electric field observations during the 2000 activity of Miyake-jima volcano, Central Japan, *Earth Planet. Sci. Lett.*, *203*, 769–666.

Satake, K., and H. Kanamori (1991), Abnormal tsunami caused by the June 13, 1984, Torishima, Japan, earthquake, *J. Geophys. Res.*, *96*(B12), 19,933–19,939.

Saunders, S. J. (2001), The shallow plumbing system of Rabaul caldera: A partially intruded ring fault?, *Bull. Volcanol.*, *63*, 406–420, doi:10.1007/s004450100159.

Saunders, S. J. (2005), The possible contribution of circumferential fault intrusion to caldera resurgence, *Bull. Volcanol.*, *67*, 57–71, doi:10.1007/s00445-004-0360-z.

Schmincke, H. U. (2004), *Volcanism*, Springer, New York.

Sekitani, H., K. Goto, H. Miyamachi, T. Kakuta, and S. Hirano (1997), Aftershock distribution of the September 9, 1996 earthquake (M_{JMA}5.7) at Tanegashima, Japan (in Japanese with English abstract), *Rep. Fac. Sci., Kagoshima Univ.*, *30*, 89–99.

Shearer, P. M. (1994), Global seismic event detection using a matched filter on long-period seismograms, *J. Geophys. Res.*, *99*, 13,713–13,735.

Shuler, A., and G. Ekström (2009), Anomalous earthquakes associated with Nyiragongo Volcano: Observations and potential mechanisms, *J. Volcanol. Geotherm. Res.*, *181*(3–4), 219–230, doi:10.1016/j.jvolgeores.2009.01.011.

Siebert, L., and T. Simkin (2002-), Volcanoes of the world: An illustrated catalog of Holocene volcanoes and their eruptions, Smithsonian Institution, Global Volcanism Program, Digital Information Series, GVP-3, http://www.volcano.si.edu/world.

Smith, G. P., and G. Ekström (1997), Interpretation of earthquake epicenter and CMT centroid locations, in terms of rupture length and direction, *Phys. Earth Planet. Inter.*, *102*, 123–132.

Smith, I. E. M., R. N. Brothers, F. G. Muiruri, and P. R. L. Browne (1988), The geochemistry of rock and water samples from Curtis Island Volcano, Kermadec Group, Southwest Pacific, *J. Volcanol. Geotherm. Res.*, *34*, 233–240.

Smithsonian Institution (1990a), Ol Doinyo Lengai, *Bulletin of the Global Volcanism Network*, *15*, 5.

Smithsonian Institution (1990b), Ol Doinyo Lengai, *Bulletin of the Global Volcanism Network*, *15*, 8.

Smithsonian Institution (1994), Rabaul, *Bulletin of the Global Volcanism Network*, *19*, 8.

Smithsonian Institution (1995a), Rabaul, *Bulletin of the Global Volcanism Network*, *20*, 2.

Smithsonian Institution (1995b), Vailulu'u, *Bulletin of the Global Volcanism Network*, *20*, 1.

Smithsonian Institution (1996a), Grimsvötn, *Bulletin of the Global Volcanism Network*, *21*, 9.

Smithsonian Institution (1996b), Rabaul, *Bulletin of the Global Volcanism Network*, *21*, 2.

Smithsonian Institution (2006), Sierra Negra, *Bulletin of the Global Volcanism Network*, *31*, 12.

Smithsonian Institution (2009), Curtis Island, *Bulletin of the Global Volcanism Network*, *34*, 2.

Sparks, R. S. J., J. Barclay, E. S. Calder, R. A. Herd, J.-C. Komorowski, R. Luckett, G. E. Norton, L. J. Ritchie, B. Voight, and A. W. Woods (2002), Generation of a debris avalanche and violent pyroclastic density current on 26 December (Boxing Day) 1997 at Soufrière Hills Volcano, Montserrat, in *The Eruption of Soufrière Hills Volcano, Montserrat, from 1995 to 1999*, edited by T. H. Druitt and B. P. Kokelaar, pp. 409–434, Geological Society, London.

Steffke, A. M., D. Fee, M. Garces, and A. Harris (2010), Eruption chronologies, plume heights and eruption styles at Tungurahua Volcano: Integrating remote sensing techniques and infrasound, *J. Volcanol. Geotherm. Res.*, *193*, 143–160, doi:10.1016/j.jvolgeores.2010.03.004.

Stix, J., and T. Kobayashi (2008), Magma dynamics and collapse mechanisms during four historic caldera-forming events, *J. Geophys. Res.*, *113*, B09205, doi:10.1029/2007JB005073.

Strelitz, R. A. (1989), Choosing the "best" double couple from a moment-tensor inversion, *Geophys. J. Int.*, *99*, 811–815.

Sugioka, H., Y. Fukao, T. Kanazawa, and K. Kanjo (2000), Volcanic events associated with an enigmatic submarine eruption, *Geophys. J. Int.*, *142*, 361–370.

Sykes, L. R. (1967), Mechanism of earthquakes and nature of faulting on the mid-oceanic ridges, *J. Geophys. Res.*, *72*(3), 2131–2153, doi:10.1029/JZ072i008p02131.

Syracuse, E. M., and G. A. Abers (2006), Global compilation of variations in slab depth beneath arc volcanoes and implications, *Geochem. Geophys. Geosys.*, *7*(5), Q05017, doi:10.1029/2005GC001045.

Takeo, M. (1990), Analysis of long-period seismic waves excited by the November 1987 eruption of Izu-Oshima Volcano, *J. Geophys. Res.*, *95*(B12), 19,377–19,393.

Talandier, J., and E. A. Okal (1987), Seismic detection of underwater volcanism: The example of French Polynesia, *Pure Appl. Geophys.*, *125*(6), 919–950.

Tedesco, D., O. Vaselli, P. Papale, S. A. Carn, M. Voltaggio, G. M. Sawyer, J. Durieux, M. Kasereka, and F. Tassi (2007), January 2002 volcano-tectonic eruption of Nyiragongo volcano, Democratic Republic of Congo, *J. Geophys. Res.*, *112*, B09202, doi:10.1029/2006JB004762.

Templeton, D. C., and D. S. Dreger (2006), Non-double-couple earthquakes in the Long Valley Volcanic Region, *Bull. Seismol. Soc. Am.*, *96*(1), 69–79, doi:10.1785/0120040206.

Tkalčić, H., D. S. Dreger, G. R. Foulger, and B. R. Julian (2009), The Puzzle of the 1996 Bárdarbunga, Iceland, Earthquake: No volumetric component in the source mechanism, *Bull. Seismol. Soc. Am.*, *99*(5), 3077–3085.

Toda, S., R. S. Stein, and T. Sagiya (2002), Evidence from the AD 2000 Izu islands earthquake swarm that stressing rate governs seismicity, *Nature*, *419*, 58–61.

Uhira, K., T. Baba, H. Mori, H. Katayama, and N. Hamada (2005), Earthquake swarms preceding the 2000 eruption of Miyakejima

volcano, Japan, *Bull. Volcanol.*, *67*, 219–230, doi:10.1007/s00445-004-0405-3.

Ukawa, M., E. Fujita, E. Yamamoto, Y. Okada, and M. Kikuchi (2000), The 2000 Miyakejima eruption: Crustal deformation and earthquakes observed by the NIED Miyakejima observation network, *Earth Planets Space*, *52*(8), xix–xxvi.

Vaughan, R. G., and P. W. Webley (2010), Satellite observations of a surtseyan eruption: Hunga Ha'apai, Tonga, *J. Volcanol. Geotherm. Res.*, *198*, 177–186, doi:10.1016/j.jvolgeores.2010.08.017.

Voight, B., J.-C. Komorowski, G. E. Norton, A. B. Belousov, M. Belousova, G. Boudon, P. W. Francis, W. Franz, P. Heinrich, R. S. J. Sparks, and S. R. Young (2002), The 26 December (Boxing Day) 1997 sector collapse and debris avalanche at Soufrière Hills Volcano, Montserrat, in *The Eruption of Soufrière Hills Volcano, Montserrat, from 1995 to 1999*, edited by T. H. Druitt and B. P. Kokelaar, pp. 363–407, Geological Society, London.

White, S. M., J. A. Crisp, and F. J. Spera (2006), Long-term volumetric eruption rates and magma budgets, *Geochem. Geophys. Geosyst.*, *7*(3), doi:10.1029/2005GC001002.

Wolfe, E. W., and R. P. Hoblitt (1996), Overview of the eruptions, in *Fire and Mud: Eruptions and Lahars of Mount Pinatubo, Philippines*, edited by C. G. Newhall and R. S. Punongbayan, pp.3–20, Univ. of Washington Press, Seattle.

Wood, C. P., I. A. Nairn, C. O. McKee, and B. Talai (1995), Petrology of the Rabaul caldera area, Papua New Guinea, *J. Volcanol. Geotherm. Res.*, *69*(3–4), 285–302.

Woods, A. W., R. S. J. Sparks, L. J. Ritchie, J. Batey, C. Gladstone, and M. I. Bursik (2002), The explosive decompression of a pressurized volcanic dome: The 26 December 1997 collapse and explosion of Soufrière Hills Volcano, Montserrat, in *The Eruption of Soufrière Hills Volcano, Montserrat, from 1995 to 1999*, edited by T. H. Druitt and B. P. Kokelaar, pp. 457–465, Geological Society, London.

Wright, R., L. Flynn, H. Garbeil, A. Harris, and E. Pilger (2002), Automated volcanic eruption detection using MODIS, *Remote Sens. Environ.*, *82*, 135–155.

Wright, R., L. P. Flynn, H. Garbeil, A. J. L. Harris, and E. Pilger (2004), MODVOLC: Near-real-time thermal monitoring of global volcanism, *J. Volcanol. Geotherm. Res.*, *135*, 29–49.

Yamamoto, E., M. Ukawa, E. Fujita, Y. Okada, and M. Kikuchi (2001), Step-like tilt change occurred during the caldera-forming stage of the 2000 Miyakejima volcanic activity (in Japanese with English abstract), *J. Geogr.*, *110*(2), 181–190.

Yamaoka, K., M. Kawamura, F. Kimata, N. Fujii, and T. Kudo (2005), Dike intrusion associated with the 2000 eruption of Miyakejima Volcano, Japan, *Bull. Volcanol.*, *67*, 231–242, doi:10.1007/s00445-004-0406-2.

Young, S. R., B. Voight, J. Barclay, R. A. Herd, J.-C. Komorowski, A. D. Miller, R. S. J. Sparks, and R. C. Stewart (2002), Hazard implications of small-scale edifice instability and sector collapse: A case history from Soufrière Hills Volcano, Montserrat, in *The Eruption of Soufrière Hills Volcano, Montserrat, from 1995 to 1999*, edited by T. H. Druitt and B. P. Kokelaar, pp. 349–361, Geological Society, London.

Yun, S., P. Segall, and H. Zebkar (2006), Constraints on magma chamber geometry at Sierra Negra Volcano, Galápagos Islands, based on InSAR observations, *J. Volcanol. Geotherm. Res.*, *150*, 232–243.

Yun, S.-H. (2007), A mechanical model of the large-deformation 2005 Sierra Negra volcanic eruption derived from InSAR measurements, PhD Thesis, Department of Geophysics, Stanford University, 125 pp.